Characterizing the diurnal cycle of South Atlantic stratocumulus cloud properties from satellite retrievals

Chellappan Seethala[1], Jan Fokke Meirink[2], Ákos Horváth[3], Ralf Bennartz[4], Rob Roebeling[5]

5   [1]Finnish Meteorological Institute, Kuopio, Finland

[2]Royal Netherlands Meteorological Institute, De Bilt, Netherlands

[3]University of Hamburg, Hamburg, Germany

[4]Vanderbilt University, Nashville, TN & University of Wisconsin – Madison, Madison, WI.

[5]EUMETSAT, Darmstadt, Germany

10   *Correspondence to*: Chellappan Seethala (seethala.chellappan@fmi.fi)

Abstract

35   Marine stratocumulus (Sc) clouds play an essential role in the earth radiation budget. Here, we compare liquid water

path (LWP), optical thickness (COT), and effective radius (CER) retrievals from two years of collocated Spinning

Enhanced Visible and InfraRed Imager (SEVIRI), MODerate resolution Imaging Spectroradiometer (MODIS), and

Tropical Rainfall Measuring Mission Microwave Imager (TMI) observations, estimate the effect of biomass burning

smoke on passive imager retrievals, as well as evaluate the diurnal cycle of South Atlantic marine Sc clouds.

40   The effect of absorbing aerosols from biomass burning on the retrievals was investigated using aerosol index (AI)

obtained from the Ozone Monitoring Instrument (OMI). SEVIRI and MODIS LWPs were found to decrease with

increasing AI relative to TMI LWP, consistent with well-known negative visible/near-infrared retrieval biases in

COT and CER. In the aerosol-affected months of July-August-September, SEVIRI LWP – based on the 1.6-µm

CER – was biased low by 14 g m^{-2} (~16 %) compared to TMI in overcast scenes, while MODIS LWP showed a

45   smaller low bias of 4 g m^{-2} (~5 %) for the 1.6-µm channel and a high bias of 8 g m^{-2} (~10 %) for the 3.7-µm channel

compared to TMI. Neglecting aerosol-affected pixels reduced the mean SEVIRI-TMI LWP bias considerably. On a

two-year data base, SEVIRI LWP had a correlation with TMI and MODIS LWP of about 0.86 and 0.94,

respectively, and biases of only 4–8 g m^{-2} (5–10 %) for overcast cases.

The SEVIRI LWP diurnal cycle was in good overall agreement with TMI except in the aerosol-affected months.

50   Both TMI and SEVIRI LWP decreased from morning to late afternoon, after which a slight increase was observed.

Terra and Aqua MODIS mean LWPs also suggested a similar diurnal variation. The relative amplitude of the two-

year mean and seasonal mean LWP diurnal cycle varied between 35–40 % from morning to late afternoon for

overcast cases. The diurnal variation in SEVIRI LWP was mainly due to changes in COT, while CER showed only

little diurnal variability.

55

1. Introduction

Changes in marine boundary layer (MBL) clouds over eastern subtropical oceans and associated differences in cloud

radiative forcing are thought to be the main source of uncertainty in climate feedback simulations (Bony and

Dufresne, 2005; Meehl et al., 2007, Zelinka et al., 2017). Climate models do not yet adequately parameterize the

60   physical and dynamical processes affecting the formation of these clouds and fail to represent their variability on

different time scales. Thus, understanding MBL cloud variability and its driving mechanisms remains crucial.

Marine stratocumulus (Sc) clouds, prevalent over eastern subtropical oceans, are vital for radiation budget

calculations because they reflect most of the incoming solar radiation back to space while having little effect on terrestrial radiation. Marine Sc clouds tend to form under relatively cold sea surface temperatures (SSTs), within a

65   shallow, well-mixed MBL capped by strong subsidence and a strong temperature inversion (e.g., Albrecht et al., 1995; Norris, 1998; Wood and Hartmann, 2006; Sandu et al., 2010). Several studies investigated the synoptic to inter-annual variability and the driving mechanisms of these clouds from both an observational and a modeling perspective (e.g., Klein and Hartmann, 1993; Klein et al., 1995; Bretherton and Wyant, 1997; Wood and Bretherton, 2006; Eastman et al., 2011; Wood, 2012; Adebiyi and Zuidema, 2015; Adebiyi and Zuidema, 2016; Horowitz et al.,

70   2017; Kar et al., 2018; Lu et al., 2018).

Marine Sc clouds are prevalent throughout the year and exhibit an explicit diurnal cycle (Minnis and Harrison, 1984; Wood et al., 2002, 2012). The daily maximum in marine Sc clouds tends to occur during the early morning hours before sunrise, while the minimum usually occurs in the afternoon (Minnis et al., 1992; Rozendaal et al., 1995; Bretherton et al., 1995; Wood et al., 2002). During daytime, shortwave absorption by clouds effectively

75   reduces or even cuts off the transport of heat and moisture from the surface into the cloud layer, resulting in a decoupled MBL (Nicholls, 1984; Betts, 1990); simultaneously, enhanced cloud-top entrainment of dry air from above promotes a weaker inversion (Duynkerke et al., 2004), which leads to thinner or even disappearing clouds. During the night, on the other hand, strong longwave radiative cooling near cloud top produces negative buoyancy and, hence, a vertically well-mixed stable MBL (James, 1957; Moeng et al., 1992; Bretherton and Wyant, 1997),

80   which increases cloud amount. Previous studies documented that subtropical Sc plays a significant role in the entire tropical response to climate perturbations (Miller, 1997), and underestimating these clouds in global climate models can lead to a positive SST bias as large as ~5 K (Ma et al., 1996). GCMs often fail to capture the diurnal variation of important processes in the cloud-topped MBL, such as the reduction of cloud fraction and the likelihood of decoupling in the afternoon (Abel et al., 2010; Medeiros et al., 2012). Wilson and Mitchell (1986) and Rozendaal et

85   al. (1995) also demonstrated that introducing, or simply altering the resolution of, the diurnal cycle of these clouds in a GCM could trigger cloud radiative forcing both at the surface and at the top-of-atmosphere. Moreover, in the Fourth Assessment Report of the Intergovernmental Panel on Climate Change Forster et al. (2007) highlighted the diurnal cycle of stratiform clouds as one of the major uncertainties in current estimates of cloud radiative forcing. Comparisons of observations with models also revealed large and potentially systematic errors in the modeled

90   diurnal cycle (O'Dell et al., 2008; Roebeling and van Meijgaard, 2009; Greuell et al., 2011).

To fully evaluate the diurnal cycle of Sc clouds, reliable observations with high spatial and temporal resolution are needed; the paucity of such data is one of the main reasons for the current level of uncertainty. A few studies took advantage of measurements available from intensive field campaigns, satellites, and model simulations to investigate the diurnal variations of these clouds. Notably, Blaskovic et al. (1990) evaluated the diurnal cycle of

95   northeast Pacific Sc off the California coast using observations during the First International Satellite Cloud Climatology Project Regional Experiment (FIRE). Most recently, Painemal (2017) evaluated the diurnal cycle of cloud entrainment rate over the northeast Pacific marine boundary layer clouds based on geostationary satellite retrievals and a mixed-layer model, and reported that the cloud top height tendency term dominates the entrainment. Ciesielski et al. (2001) evaluated the diurnal variation of northeast Atlantic Sc from the Atlantic Stratocumulus

100   Transition Experiment (ASTEX). Zuidema and Hartmann (1995) and Wood et al. (2002) studied the diurnal variation in liquid water path (LWP) based on observations from microwave imagers. Rahn and Garreaud (2010) and Burleyson et al. (2013) evaluated the diurnal cycle of southeast Pacific Sc using the Variability of the American Monsoon Systems' Ocean-Cloud-Atmosphere-Land Study Regional Experiment (VOCALS-REx) datasets. Kniffka et al. (2014) studied the temporal and spatial characteristics of LWP of different types of clouds from SEVIRI data,

105   for most of Europe and Africa. In general, all of these studies revealed an early morning maximum and afternoon minimum in cloud amount and LWP, linked to solar insolation/absorption. Rozendaal et al. (1995) and Wood et al. (2002) showed that the amplitude of diurnal variations in cloud amount and LWP could exceed 20 % of the mean value. These studies, however, did not consider diurnal variations in cloud optical thickness (COT) or droplet effective radius (CER) and were usually based on limited measurements from a single instrument, the uncertainties

110   of which were not well characterized. Painemal et al. (2012) evaluated the diurnal cycle of LWP, COT, and CER for southeast Pacific Sc based on GOES-10 (Geostationary Operational Environmental Satellite-10) and microwave observations, but only for a period of two months. They noted that variations in COT drive the diurnal cycle of LWP mostly.

In this study, we investigate the diurnal variations of southeast Atlantic Sc clouds. The southeast Atlantic

115   domain is notable for its unique feature that part of the year a smoke layer transported from the continent resides above the Sc clouds, which poses a challenge to the retrieval of aerosol and cloud properties from space. In recent years several field campaigns have been initiated as described in Zuidema et al. (2016), to investigate aerosol-cloud interactions and their role in climate. The purpose of our study is three-fold. One, to compare the Meteosat Second Generation (MSG) Spinning Enhanced Visible and InfraRed Imager (SEVIRI) CLoud property dAtAset using

120   SEVIRI - Edition 2 (CLAAS-2) from the Satellite Application Facility on Climate Monitoring (CM SAF) (Benas et

al., 2017) against Version 7 TMI (Tropical Rainfall Measuring Mission (TRMM) Microwave Imager) (Wentz 2018)

and Collection 6 MODIS (Moderate Resolution Imaging Spectro-radiometer) retrievals (Platnick et al., 2017). Two,

to quantify the effect of above-cloud aerosols on LWP retrievals from the SEVIRI and MODIS passive imagers.

Three, to study the diurnal cycle of Sc clouds in the South Atlantic, which is a somewhat neglected region as most

125   previous studies focused on the North or South Pacific (west of California and Chile). The main strength of our

study is the use of an extensive two-year dataset, which allows us to investigate the seasonal variation of the diurnal

cycle. SEVIRI's higher temporal resolution of 15 minutes allows examining the diurnal cycle with greater detail

than offered by earlier GOES instruments. We only consider non-raining warm liquid clouds to avoid significant

retrieval uncertainties associated with the presence of rain and ice clouds at higher altitudes. Retrieval artifacts

130   related to absorbing aerosols (e.g., Haywood et al., 2004) have been evaluated and aerosol-affected grid boxes have

subsequently been removed from the analysis.

      The paper is structured as follows. A description of our datasets including retrieval artifacts and

uncertainties is provided in Section 2. The comparison methodology is described in Section 3. Section 4 discusses

retrieval biases related to the presence of smoke from continental biomass burning over clouds and analyzes spatial

135   distributions, comparison statistics, and diurnal variations of Sc properties from SEVIRI, TMI, and Terra and Aqua

MODIS on seasonal and two-year timescales. Finally, a summary is offered in Section 5.

2. Satellite datasets

2.1 Visible/Near-infrared (VIS/NIR) retrievals

140   **2.1.1 Spinning Enhanced Visible and InfraRed Imager (SEVIRI)**

SEVIRI is an optical radiometer onboard the MSG geostationary satellite series operated by the European

Organization for the Exploitation of Meteorological Satellites (EUMETSAT). SEVIRI measures radiances in 12

spectral bands including 4 VIS/NIR channels (0.6–1.6 µm plus a broadband high-resolution VIS channel) and 8 IR

channels (3.9–13.4 µm). It has a spatial resolution of 3x3 km^2 at nadir and a repeat frequency of 15 minutes for full-

145   disk images covering Europe, Africa, and the Atlantic Ocean.

      The CM SAF CLAAS-2 climate data record is described in Benas et al. (2017). Part of the cloud

processing software is the CPP (cloud physical properties) algorithm, which retrieves cloud optical thickness and

cloud particle effective radius based on measured reflectances in the 0.6-µm and 1.6-µm channels. The retrieval

scheme is based on earlier bispectral methods (hereafter also referred to as visible/near-infrared or VIS/NIR

150 technique) that retrieve cloud optical thickness and cloud particle size from satellite radiances at wavelengths in the

(for clouds) non-absorbing visible and the moderately absorbing solar infrared part of the spectrum (Nakajima and

King 1990; Han et al. 1994; Nakajima and Nakajima, 1995; Watts et al., 1998; Roebeling et al., 2006]. The liquid

water path is computed from the retrieved optical thickness (τ or COT) and droplet effective radius (r_e or CER) as

$$LWP = \frac{2}{3}\,\tau r_{e(1.6\mu m)}\rho_l, \text{ where } \rho_l \text{ is the density of liquid water (Stephens 1978).} \qquad (1)$$

155 The SEVIRI retrievals are available only during daytime and are performed assuming plane parallel clouds. Because

r_e is not well constrained by the measured 1.6-μm channel reflectance for thin clouds, it is weighted towards a

climatological a priori value of 8 μm for pixels with $\tau \leq 4$ -similar to the handling of small optical thicknesses in

optimal estimation methods. The relationship used to weight the CER retrieval is,

$$r_{e,assign} = r_{e,clim}\,(1-w) + r_{e,ret}\,w \qquad (2)$$

160 where, $w = 1/(1 + e^{(-1.25(\tau_{ret}-\tau_{w,clim}))})$, $r_{e,clim} = 8$ micron; $\tau_{w,clim} = 2.5$

In part of our analysis, a $\tau > 3$ threshold is applied to minimize the impact of strongly weighted effective radii for

thin clouds on the results. The SEVIRI shortwave channels were calibrated with Aqua-MODIS as described in

Meirink et al. (2013). More details on the CPP retrieval algorithm are provided in CM SAF (2016).

165 **2.1.2 Moderate Resolution Imaging Spectroradiometer (MODIS)**

MODIS is the flagship instrument aboard the Terra and Aqua polar orbiter satellites. Terra has a 10:30am

descending node sun-synchronous orbit, while Aqua has a 13:30pm ascending node sun-synchronous orbit. Terra

and Aqua MODIS image the entire Earth's surface every 1 to 2 days, acquiring data in 36 spectral bands. The

MODIS Collection 6 (C6) cloud property datasets (Platnick et al., 2017) with 1x1 km^2 spatial resolution from both

170 Terra (MOD06) and Aqua (MYD06) have been used in this study.

Similar to CLAAS-2 SEVIRI, the MODIS C6 algorithm uses the VIS/NIR technique to retrieve cloud

properties. Over ocean, the 0.86-μm band is used for optical thickness information in conjunction with one of three

water-absorbing near-infrared bands located at 1.6, 2.2, and 3.7-μm, which are particularly sensitive to droplet

effective radius. Although all three near-infrared channels generally observe the upper portion of clouds, the vertical

175 sampling of droplets becomes progressively deeper from 3.7 to 1.6-μm due to decreasing absorption (Platnick,

2000).

The C6 algorithm is a revamped version of the Collection 5 (C5) algorithm that has gone through several

updates to improve performance. Modifications include improved radiative transfer and lookup tables with finer

COT and CER bins, redesigned cloud thermodynamic phase detection based on a variety of independent tests, and

180   separate spectral retrievals of COT, CER, and derived LWP for channel combinations using the 1.6, 2.2, and 3.7-μm

bands. Differences in CER between C5 and C6 are evaluated in Rausch et al. (2017). Depending on a subpixel

heterogeneity index, the properties of partly cloudy pixels are listed separately and the algorithm also provides

retrieval failure metrics for pixels where the observed reflectances fall outside the LUT solution space.

185   **2.1.3 Known retrieval artifacts in VIS/NIR retrievals**

While these datasets offer excellent resources for investigating warm, overcast single-layer clouds, they are subject

to certain retrieval artifacts due to algorithm assumptions and complexities in the retrieval technique. The VIS/NIR

cloud property retrievals rely on 1-D radiative transfer model-generated LUTs, which do not account for subpixel

cloud heterogeneity and 3-D cloud structure, and that could lead to significant biases in retrieved cloud properties

190   for inhomogeneous and partially cloudy scenes. Cloud vertical stratification is essential to consider when computing

LWP. Although MODIS retrieves effective radius at three separate water-absorbing channels, 1.6, 2.2, and 3.7-μm,

all three are most sensitive to near cloud-top properties (Platnick 2000; Zhang and Platnick 2011). Hence, the LWP

derived by combining retrieved τ and retrieved r_e from any one of the near IR channels could potentially under- or

overestimate the true value depending upon the actual cloud stratification. For stratocumulus that typically follows a

195   sub-adiabatic r_e profile, bigger droplets will be located near cloud top, and thus the derived LWP could be an

overestimate. As a first-order correction, an adiabatic model is proposed by Wood and Hartmann (2006), which

results in a ~17% reduction from the standard vertically homogeneous LWP in eq. 1 (Bennartz 2007; Bennartz and

Rausch, 2017). More details about the retrieval uncertainties of the VIS/NIR technique can be found in Horváth and

Davies (2007), Seethala and Horváth (2010), Horváth et al. (2014), Zhang et al., (2012), Grosvenor et al., (2018) and

200   references therein.

2.2 TRMM Microwave Imager (TMI)

TMI was a 5-channel, dual-polarized, passive microwave imager onboard the Tropical Rainfall Measuring Mission

(TRMM) satellite that was operational between December 1997 – April 2015, TMI continuously monitoring the

205   tropics between 40° S and 40° N. Unlike the sun-synchronous polar orbiters hosting the similar SSM/I (Special

Sensor Microwave/Imager) instruments, the TRMM satellite precessed west to east in a semi-equatorial orbit,

producing data at different local times. The radiometer measured microwave radiation at 10.7, 19.4, 21.3, 37, and

85.5 GHz. The Wentz absorption-emission based algorithm (Wentz, 1997; Wentz and Spencer, 2000; Hilburn and

Wentz, 2008) is used to retrieve meteorological parameters such as sea surface temperature (SST), surface wind

210   speed (W), water vapor path (V), liquid water path (LWP), and rain rate (R) over the ocean. Our primary interest,

LWP, is mainly derived from 37-GHz observations at a native resolution of 13 km, although here we used the 0.25°

gridded product available from Remote Sensing Systems (RSS). The error characteristics of TMI data are similar to

those of the RSS SSM/I and AMSR-E (Advanced Microwave Scanning Radiometer for Earth Observing System)

products, as all microwave retrievals are produced by the same unified algorithm. Various sources of potential errors

215   are documented in Horváth and Gentemann (2007), O'Dell et al. (2008), Seethala and Horváth (2010), Elsaesser et

al. (2017), and Greenwald et al. (2018). Because the diurnal cycle is targeted here, the non-sun-synchronous TMI

observations are particularly useful. The precessing orbit of TRMM allows for a comparison of observations at

different local times, which cover the entire diurnal cycle over the course of a month.

TMI data were recently reprocessed using the significantly improved version 7 (V7) of the radiometer data

220   processing algorithm (Wentz, 2015). The following major modifications were introduced: TMI brightness

temperatures were recalibrated using the same procedures applied to all other RSS microwave products, the

previously removed small negative LWP values are now reported, some large geolocation errors were corrected, the

roll of the satellite was recalculated, the radiation contribution from the emissive antenna itself was removed, and

Radio Frequency Interference (RFI) from the cold mirror was minimized. This improved V7 TMI product available

225   at www.remss.com was utilized in this study.

2.3 Ozone Monitoring Instrument (OMI)

Areas affected by biomass burning smoke or desert dust were identified using OMI ultraviolet Aerosol Index (AI).

OMI AI represents the deviation of measured 354-nm radiance from model estimates calculated for a purely

230   molecular atmosphere bounded by a Lambertian surface, with positive values indicating the presence of absorbing

aerosols (Torres et al. 2007). A distinguishing feature of OMI AI is its ability to detect absorbing aerosols above

(and even mixed with) clouds. Specifically, we used the 0.25° resolution daily Level-2 gridded product

(OMAERUVG).

235   **3. Comparison methodology**

For our study we used two years of data (December 2010 – November 2012) from SEVIRI, TMI, and Terra- and

Aqua-MODIS. We consider JJA (June-July-August), SON (September-October-November), DJF (December-

January-February), and MAM (March-April-May) respectively to represent austral winter, spring, summer, and autumn; henceforth, 'seasonal' refers to an average over a given season in 2 consecutive years. SEVIRI pixel-level

240   data were averaged down to TMI's 0.25^o x 0.25^o resolution, only using SEVIRI retrievals within ±7.5 minutes of the TMI observation time. Note that SEVIRI LWP is representative of the in-cloud LWP. For compatibility with the TMI gridbox-mean LWP, we multiplied SEVIRI LWP with the successful cloud retrieval fraction (henceforth referred to as "liquid cloud fraction" or LCF) within the TMI gridbox. Similarly, when matching COT, CER, and LWP from SEVIRI and MODIS, both datasets were averaged down to 0.25^o x 0.25^o resolution, using the same

245   temporal collocation criterion of ±7.5 minutes.

Our study domain is a 70° x 40° (50° W-20° E, 35° S-5° N) area in the Southeast Atlantic. Over the relatively cold SSTs near the Namibian coast extensive sheets of marine Sc clouds form, which transition into scattered trade Cu as they are advected towards the warmer ocean near the equator. Decks of subtropical marine Sc, scattered Cu, and occasionally deep convective clouds cover the study domain. We however restricted our analysis to marine Sc

250   clouds.

Because microwave and optical techniques represent fully independent approaches, each having their own shortcomings, the analysis of retrieval discrepancies does not necessarily establish absolute accuracies. A considerable number of studies have investigated the differences between LWP retrievals based on passive microwave and VIS/NIR satellite observations (Bennartz, 2007; Borg and Bennartz, 2007; Horváth and Davies,

255   2007; Horváth and Gentemann, 2007; Wilcox et al., 2009; Greenwald, 2009; Seethala and Horváth, 2010; Horváth et al., 2014, Cho et al., 2015; Greenwald et al., 2018). The major shortcomings of microwave measurements were found to be the uncertain retrieval of LWP in the presence of rain and a wet (positive) bias of 10-15 g m^{-2} in broken cloud fields. However, V7 TMI data now includes the small negative LWP values that were previously discarded, and thus the microwave wet-bias has been significantly reduced (Greenwald et al., 2018).

260   The major issues affecting VIS/NIR measurements are the dependence of retrievals on cloud fraction, variations with sun-view geometry, horizontal and vertical inhomogeneity causing 3D radiative effects, and the presence of aerosols/cirrus above the liquid cloud layer. Agreement between the VIS/NIR and microwave techniques is generally better for more stratiform clouds, where a near-adiabatic cloud liquid water profile can be assumed. To minimize these retrieval problems, we examine the diurnal characteristics of only low-level non-

265   raining warm (liquid) clouds, which typically dominate the South Atlantic marine Sc domain. Additional criteria are applied to reduce as much as possible the influence of rain and ice clouds -grid boxes are included only if flagged as

confident liquid clouds with valid LWP retrieval, and cloud top temperature (CTT) > 275 K in SEVIRI and MODIS

retrievals with ice fraction ≤ 0, and, rain rate ≤ 0 in TMI retrievals. Our study domain is also affected by continental

biomass burning during austral winter and spring, which in turn affects VIS/NIR cloud retrievals, therefore, special

270   attention is paid to the analysis of retrieval artifacts related to the presence of smoke over the Sc deck.

We noticed that the extent and location of South Atlantic Sc clouds vary from month to month; hence we

opted to define the Sc domain dynamically, rather than selecting a fixed rectangular area to specify the study

domain. Thresholding the spatial mean map of liquid cloud fraction (LCF) and the heterogeneity parameter ($H_σ$ =

reflectance standard deviation / mean reflectance) was found to delineate Sc regions in good agreement with visual

275   observations. To precisely define the Sc domain, we used a region-growing algorithm to find adjacent, connected

grid-boxes with LCF > 80 %. The identified Sc regions were typically within 20° W – 20° E and 5° – 35° S. Cloud

properties were separately evaluated for two cases:

1. 'all-sky': including all grid boxes in the identified Sc domain.

2. 'overcast': only including grid boxes with LCF ≥ 95 % and COT > 3 in the identified Sc domain.

280   These criteria were imposed to minimize retrieval artifacts related to broken clouds as well as thin

clouds for which the CER retrieval in particular is relatively uncertain.

4. Results and Discussion

4.1 Effect of biomass burning smoke on SEVIRI and MODIS retrievals

285   This section presents the analysis of the effect of smoke and/or aerosols above marine Sc on passive VIS/NIR

imager retrievals of cloud properties. Our study domain, especially the Sc region located off the Namibia coast, is

severely influenced by biomass burning on the African continent, as it produces episodic plumes of dark smoke that

drift over the southeast Atlantic Ocean during the dry season JJASO (June-through-October). Beneath the elevated

smoke layer, there is a persistent deck of bright marine Sc clouds. Previous research (Hobbs, 2002; McGill et al.,

290   2003; Wilcox, 2010) has shown that the smoke is typically located in layers (at 2 to 4 km altitude) that are vertically

separated from the Sc clouds below (at ~1.5 km altitude) and, hence, direct microphysical interaction between the

aerosols and the Sc is often inhibited by the strong temperature inversion above the cloud layer. However, more

recent studies e.g., Rajapakshe et al. (2017) reported that smoke layers are closer to the cloud layer, and significantly

enhance the brightness of stratocumulus over there (Lu et al. 2018). Recently, several studies evaluated the

295   dynamical and climatological impacts of the presence of smoke above Sc clouds from both modeling as well as

satellite and/or field campaign measurements (Adebiyi et al., 2015; Adebiyi and Zuidema, 2016; Zuidema et al.,

2016; Das et al., 2017; Horowitz et al., 2017; Chang and Christopher, 2017; Lu et al., 2018; Kar et al., 2018). When

smoke resides above low-level clouds, the observed visible channel (0.6- or 0.8-µm) reflectance is reduced due to

absorption by smoke, which is not taken into account in the LUTs and can introduce a negative bias in the retrieved

300   COT as well as CER, and hence in LWP. According to Haywood et al. (2004), this negative bias in the 1.6-µm CER

is significantly larger than that in the 2.1-µm CER (which is estimated to be less than 1 µm), while the bias in

retrieved COT can be up to 30 %. Previous studies also noticed a domain-mean underestimation of ~3 to 6 g m^{-2} in

MODIS LWP over the South Atlantic Sc region in the presence of absorbing aerosols (Bennartz and Harshvardhan,

2007; Wilcox et al., 2009; Seethala and Horváth, 2010). Therefore, we need to quantify the impact of absorbing

305   aerosols on SEVIRI and MODIS VIS/NIR retrievals in our Sc domain for our study period. The presence of

absorbing aerosols can be diagnosed using the OMI Aerosol Index (AI), because large positive AIs correspond to

absorbing aerosols, such as dust and smoke, and small positive or negative AIs correspond to non-absorbing

aerosols and clouds.

Figure 1a depicts the spatial distribution of average OMI aerosol index during JAS for 2011 and 2012, with

310   the black contour representing the Sc region. It is clear that absorption by smoke is highest near the Namibian coast

and decreases away from shore. The locations of greater cloud amount partly coincide with the locations of larger

AIs. The spatial distribution of SEVIRI and TMI LWP and their bias for overcast conditions are shown in Figs. 1b-

d. Near the coast where the smoke absorption is stronger, SEVIRI LWPs increasingly underestimated the TMI

LWPs (SEVIRI values were approximately half of the corresponding TMI values). Over the smoke-free areas of the

315   stratocumulus region, on the other hand, SEVIRI-retrieved LWPs were slightly higher than TMI LWPs. The

domain-mean TMI LWP is 85 g m^{-2}, whereas the mean SEVIRI LWP is only 71 g m^{-2}, indicating an LWP low bias

of 14 g m^{-2} or ~16 % in SEVIRI retrievals.

In Fig. 2, cloud properties from TMI, SEVIRI, and MODIS retrievals are binned into AI bins of 0.5 for the

overcast Sc conditions. In the SEVIRI 1.6-µm CER retrievals, a steady and strong decrease from 11 to 6 µm is

320   observed, while the COT decrease is weaker from 10.8 to 9 with AI increasing from 0 to 3.5. As a result, SEVIRI

LWP sharply decreases from 86 to 45 g m^{-2} over the same AI range. TMI LWP, in contrast, increases from 84 to 101

g m^{-2} between clean and increasingly polluted regions. For overcast grid boxes with little to no smoke absorption

(AI < 0.5), SEVIRI LWP agrees well with TMI LWP, having only a 2 g m^{-2} high bias. However, SEVIRI has a low

bias of 6–25 g m^{-2} for moderate AI between 1 and 2, and a large negative bias > 40 g m^{-2} for grid-boxes with AI >

325   2.5; the bias increases linearly with AI.

Considering that cloud amount happens to be spatially correlated with AI and that microwave retrievals are

unaffected by absorbing aerosols, the increase in TMI LWP with increasing AI, that is closer to shore, seems

plausible. Because the variability of LWP is mostly controlled by COT rather than CER in the absence of smoke-

induced retrieval biases (Seethala and Horváth, 2010; Painemal et al., 2012), the microwave retrievals suggest that

330   the true COT should also increase with AI. Taken together, the microwave and VIS/NIR retrievals imply that

SEVIRI COT is increasingly underestimated as AI increases. The low bias in SEVIRI LWP in smoke-affected areas

arises from the combination of the negative COT and CER retrieval biases. A similar underestimation is reported in

aircraft retrievals of COT and CER for a stratus deck residing below an absorbing aerosol layer (Coddington et al.,

2010).

335   Interestingly, a systematic overall increase in LWP with AI as indicated by TMI LWP in Fig. 2a was also

noticed in previous observational and modeling studies, e.g., Johnson et al. (2004), Wilcox (2010), Randles and

Ramaswamy (2010), Adebiyi et al. (2015), Adebiyi and Zuidema (2016). While this could partly be explained by the

fortuitous spatial correlation between higher aerosol loads and thicker clouds in this Sc region, these studies argue

that strong atmospheric absorption by the smoke warms the 700 hPa air temperature and increases upward motion.

340   This increased buoyancy inhibits cloud-top entrainment and promotes a stronger inversion, thereby helping to

preserve humidity and cloud cover in the MBL, resulting in increased cloud amount and LWP compared to a smoke-

free environment. Similar to our SEVIRI results, Bennartz and Harshvardhan (2007), Wilcox et al. (2009), and

Seethala and Horváth (2010) also noted a systematic MODIS LWP underestimation in Sc off southern Africa during

the biomass burning seasons. Painemal et al. (2014) also noted a CER decrease in MODIS data despite increased

345   LWP north of 5° S during the biomass burning season.

Retrieval discrepancies due to the presence of absorbing aerosols above Sc clouds were also evaluated

between SEVIRI and MODIS. Frequency histograms of SEVIRI minus MODIS LWP, COT, and CER biases, as

well as, the biases relative to MODIS CPP for overcast conditions aggregated for JAS 2011 and JAS 2012 are

shown in supplemental Fig. S1. SEVIRI COT appeared to be biased low by ~1 compared to MODIS. Compared to

350   the 1.6-μm MODIS CERs, ~70 % of SEVIRI CERs have a mean bias of -1.5 μm. Although SEVIRI CERs are

biased low compared to all three MODIS CERs, the ~1 μm additional high bias relative to the 2.1- and 3.7-μm

CERs likely indicates much smaller smoke-induced retrieval artifacts in these two channels. In general, the CER

Atmos. Chem. Phys. Discuss., https://doi.org/10.5194/acp-2018-445
Discussion started: 17 May 2018
© Author(s) 2018. CC BY 4.0 License.

Atmospheric
Chemistry
and Physics
Discussions

retrievals from SEVIRI tend to be lower than corresponding retrievals from the three MODIS channels, with SEVIRI having about 1.5 µm to 2.5 µm lower CER values. The SEVIRI minus MODIS LWP distributions peak at

355   about -10 g m^{-2} irrespective of the MODIS channel used for the retrieval.

The mean MODIS LWPs are 80 g m^{-2}, 87 g m^{-2}, and 90 g m^{-2} respectively for 1.6-, 2.1-, and 3.7-µm channel retrievals, while the corresponding mean SEVIRI LWP is 71 g m^{-2}. As shown in Fig. 2a, MODIS 1.6-µm retrieved LWP shows the largest decrease from 92 to 72 g m^{-2} with AI. In clean cases, MODIS 1.6-µm LWP is 10 % higher than the SEVIRI 1.6-µm LWP and the difference between MODIS and SEVIRI LWP is even larger for the

360   2.1- and 3.7-µm channel retrievals.

A decrease from 12 to 9 µm is observed in MODIS 1.6-µm CER, whereas both the MODIS 2.1- and 3.7-µm CERs show a smaller decrease of ~1.5 µm (Fig. 2e) with increasing AI. This, again, indicates the reduced effect of absorbing aerosols on 2.1- and 3.7-µm reflectances. Surprisingly, SEVIRI 1.6-µm CERs are about 1.5 µm (2.5 µm and 3 µm) lower than MODIS 1.6-µm (2.1- and 3.7-µm channels) CERs, even in unpolluted overcast conditions.

365   MODIS COT decreased slightly until AI < 1.5, increased steeply until AI = 2.5, and then leveled-off in all three channels. However, SEVIRI and MODIS COTs differ by 1 with MODIS being higher even in grid-boxes unaffected by smoke. Taken together both COT and CER variations, MODIS LWPs show a decreasing trend with AI in all three channels, with the largest decrease of ~20 g m^{-2} seen in the 1.6-µm retrieval. The 2.1- and 3.7-µm MODIS LWPs show a reduction of only ~10 g m^{-2}. The SEVIRI minus MODIS differences in LWP, COT, and CER

370   increased with AI even in the common 1.6-µm channel; although differences were the smallest in this channel, especially for CER. This is somewhat surprising, considering that the CLAAS-2 SEVIRI and MODIS C6 COT-CER retrieval algorithms are rather similar, the SEVIRI 1.6-µm channel has been calibrated with the corresponding MODIS channel, and the comparison is done for the most favorable overcast condition. The finding that AI has a stronger impact on SEVIRI 1.6-µm LWP than on MODIS 1.6-µm LWP may partially be explained by the spectral

375   difference that for SEVIRI retrievals the 0.6-µm channel is used as a non-absorbing channel in contrast to the 0.8-µm channel for MODIS, the latter of which is less affected by aerosol absorption.

Because the presence of absorbing aerosols above Sc clouds introduces a large negative bias in both SEVIRI and MODIS COT and CER retrievals, in the remainder of this work we will exclude grid-boxes with AI>0.1.

380

4.2 Spatial distribution and mean statistics of SEVIRI, MODIS, and TMI cloud properties

This section presents the results of the comparison of SEVIRI, MODIS, and TMI LWP retrievals, as well as the comparison of SEVIRI and MODIS COT and CER retrievals. Significant variation in the distribution and amount of clouds is observed over the Sc region from month to month. During SON, we observe frequent Sc clouds with large spatial extent. During JJA there are relatively fewer clouds that are shifted slightly to the north. The lowest cloud fractions are seen during DJF and MAM. From a surface-based cloud climatology, Klein and Hartmann (1993) also showed that there is strong seasonal variability in the amount of Sc clouds, which is closely tied to the seasonal cycle of static stability. Over the South Atlantic Sc region, SON had the largest lower tropospheric stability (LTS), and DJF had the smallest. The strongest net cloud radiative effect also occurred during August through November, which further motivates us to examine the seasonal variability of these clouds.

The spatial distributions of two-year-mean SEVIRI cloud properties and TMI LWP for the overcast condition are shown in Fig. 3, whereas the results for the all-sky case are shown in Fig. S3. In the all-sky case, the spatial distribution of LWP indicates that over the marine Sc region the measurement techniques show good agreement with negligible bias, while the two-year mean SEVIRI LWP is much lower than the corresponding TMI mean LWP in regions with generally lower cloud fractions. This is mostly due to a high bias in TMI LWP in broken scenes (Greenwald et. al., 2018). In the Sc region, SEVIRI COT varies from 6 to 11 and CER ranges between 8 and 14 μm. The two-year-mean liquid cloud fraction varies between 75 % and 100 %. The mean statistics also show robust skill in LWP retrieval for both SEVIRI and TMI with a high correlation of 0.89 for the Sc regime. Both TMI and SEVIRI show a mean LWP of ~53 g m^{-2} with negligible bias and standard deviation of 24 g m^{-2} for the study period.

In the overcast case over the Sc regime, the two-year mean LWP increases to 84 g m^{-2} and 80 g m^{-2} respectively for SEVIRI and TMI, i.e., the mean SEVIRI LWP is about 5 % larger than the mean TMI LWP. In this case, applying an adiabatic correction to SEVIRI LWP would lead to a larger bias of -10 g m^{-2} (-12 %) and standard deviation of 28 g m^{-2}. The unbiased LWP observed in the all-sky Sc case could be associated with the cancellation of errors between fully overcast and lower LCF grid-boxes within the domain. A higher mean COT of ~11 characterizes the overcast Sc case, whereas the mean COT is only about 7 in the all-sky case, suggesting the presence of optically thin clouds which are more prone to retrieval biases. Figure 4 shows a density scatterplot of TMI and SEVIRI LWPs in the overcast Sc region. Most data points are close to the one-to-one line, although at the lower end TMI LWP is slightly higher, while the reverse is true at the higher end -the same feature is also found in

monthly and seasonal results.

The daytime-averaged two-year and seasonal statistics of SEVIRI and TMI LWP are listed in Table 1. Seasonally, in the overcast Sc domain, the average LWP varies from 73 to 92 g m^{-2} in standard SEVIRI, 61 to 76 g m^{-2} in adiabatic SEVIRI, and 73 to 82 g m^{-2} in TMI retrievals. In the aerosol-free seasons of DJF and MAM,

415   standard SEVIRI overestimates TMI LWP; applying an adiabatic correction to SEVIRI in these months brings the LWP bias within 5 %, similar to previous studies. The standard SEVIRI likely overestimates the actual LWP in the overcast Sc regime due to the overestimation of CER, as the observed CER in the 1.6-μm channel corresponds to the top layer and is higher than the cloud layer-mean in sub-adiabatic stratocumulus. However, for JJA, when all three months were heavily affected by smoke aerosol, the standard SEVIRI already shows ~10 % lower LWP than TMI;

420   therefore, applying the adiabatic correction would only enhance this negative bias. For SON, only September was heavily affected by aerosol for the analysis years we considered. As a result, the mean standard SEVIRI LWP was ~5 % larger than TMI LWP and applying adiabatic correction would lead to a ~14 % underestimation in SEVIRI LWP. We found that SEVIRI underestimates LWP more during the aerosol-affected months, even after excluding grid-boxes with AI > 0.1 Applying a stricter criteria by excluding grid-boxes with AI > 0 did not improve the

425   results, hinting at OMI AI retrieval biases.

The spatial distribution of SEVIRI and MODIS cloud properties averaged for the study period for the overcast condition is shown in Fig. S5. In general, over the overcast Sc regime, MODIS retrieves higher LWPs in all three channels compared to SEVIRI, but for more broken scenes MODIS values are lower than SEVIRI LWP. The observed two-year-mean COT in the overcast Sc regime is 10.2 for SEVIRI, whereas it is 11.2 for MODIS,

430   indicating SEVIRI mean COT is about 9 % lower than MODIS mean COT. Similarly, the observed two-year-mean CER in the overcast Sc domain is 10.1 μm for SEVIRI, but for MODIS it varies between 11.3 – 11.7 μm depending on the absorption channel, indicating that SEVIRI mean CER is 11–12 % lower than MODIS CER. The lower SEVIRI LWP value over the Sc regime is due to the combination of lower COT and lower CER values compared to MODIS.

435   The higher SEVIRI LWP values in broken scenes are exclusively due to a 2–4 μm overestimation in CER compared to MODIS, as SEVIRI COTs remain underestimated in these clouds similar to overcast clouds. This overestimation could be caused by, in thin clouds with COT < 4, the SEVIRI CPP algorithm weighing CER with an a priori (climatological) value of 8 μm, but MODIS providing smaller retrieved values. Also note that the SEVIRI CER overestimation in broken clouds systematically increases as the sampling height of the comparison MODIS

440   channel gets closer to cloud top, i.e. moving from the 1.6 μm to the 3.7 μm band. This could indicate a vertically decreasing CER profile, sometimes seen in raining/drizzling small Cu clouds, in which case the cloud-top CER value, especially from the 3.7-μm band, would underestimate the cloud layer-mean, leading to a corresponding underestimation in LWP as well.

       The daytime-averaged two-year and seasonal statistics of SEVIRI and MODIS LWP re listed in Table 2,

445   whereas the respective mean COTs and CERs are listed in Table S1. For overcast marine Sc clouds the two-year mean LWP is 80 g m^{-2} for SEVIRI, 84 g m^{-2} for MODIS 1.6-μm, 88 g m^{-2} for MODIS 2.1-μm, and 87 g m^{-2} for MODIS 3.7-μm channels. The differences in retrieved LWP values vary from 4 to 8 g m^{-2} (5–10 %), whereas the differences in root mean square deviation (RMSD) values vary between 16–20 g m^{-2}. The SEVIRI and MODIS LWP retrievals are highly correlated, with correlations > 0.9. In the aerosol-unaffected seasons of DJF and MAM,

450   the difference between SEVIRI and MODIS LWPs is within 0–5 %. In the heavily polluted months of JJA, LWP retrievals from SEVIRI are about 10 % lower than those from the MODIS 1.6-μm and 20 % lower than those from the MODIS 3.7-μm band. This suggests that SEVIRI retrievals are more strongly affected by the presence of absorbing aerosols in the Sc regime than the corresponding MODIS 1.6-μm retrievals and that these polluted scenes are not sufficiently filtered out by the OMI AI threshold. Indeed, unlike in other seasons, in JJA MODIS LWP$_{1.6\text{-}\mu m}$ <

455   MODIS LWP$_{2.1\text{-}\mu m}$ < MODIS LWP$_{3.7\text{-}\mu m}$, hinting at the influence of absorbing aerosols on MODIS LWP retrievals as the 3.7-μm channel is known to be the least affected by smoke. In SON, since September is the only month strongly affected by aerosols, the comparison of SEVIRI and MODIS LWPs is better, with SEVIRI low biases of 6–12 %.

       Figure 5 shows the density scatterplots of SEVIRI versus MODIS LWPs, COTs, and CERs in the overcast Sc region for the study period. Most data points are close to the one-to-one line, but with a SEVIRI low bias; the

460   same feature is also found in monthly and seasonal results. A low COT bias of 1 compared to all three MODIS channels, and a low CER bias of 1 μm compared to MODIS 1.6-μm and a low CER bias of 1.5 μm compared to MODIS 2.1-μm and 3.7-μm bands are observed in SEVIRI overcast retrievals. The frequency histograms of SEVIRI minus MODIS CPP difference, as well as the differences with respect to different MODIS channels are shown for the all-sky case in Fig. S4 and for the overcast case in Fig. S6. The peak of the LWP absolute difference as well as

465   the relative difference distribution is centred on zero, although the distribution is negatively skewed. Interestingly, in the all-sky case ~40% of the data have shown negligible difference (zero LWP bias bin), whereas only about 30 % of the data have shown a negligible difference in the overcast case. Histograms of both COT and CER differences reveal that the distribution is off centered. Histograms of COT differences reveal a narrow distribution, which peaks

470 at -1 in the overcast case; however, in the all-sky case there is a broader peak between -1 and 0. Histograms of CER differences reveal wider distributions, especially when compared against the 2.1- and 3.7-μm channels, which peak at -1 μm in the overcast case; however, in the all-sky case the peak is again broader between -2 and -1 μm.

4.3 Diurnal cycle of SEVIRI, TMI, and MODIS cloud properties

Figures 6-7 and S7-S9 show the two-year mean and seasonal diurnal cycle of Sc cloud properties. The diurnal cycles

475 shown here are limited to cases with AI values lower than 0.1, in order to minimize VIS/NIR retrieval biases due to biomass burning smoke (see section 4.1). Because SEVIRI retrievals (black standard and green adiabatic) are only available during daytime, TMI LWP is shown separately for day (red) and night (gray) observations, which combined depict the entire 24-hour diurnal cycle. As before, the analysis is done separately for the all-sky case (solid lines with open circles) and the overcast case (dash-dotted lines with plus signs). MODIS Terra and Aqua

480 values at 10h LST and 14h LST, respectively, are plotted as symbols (open circles or plus signs) in both cases, with color (orange, light blue, yellow) indicating the water-absorbing channel used.

    For the two-year means (Fig. 6), both TMI and SEVIRI indicate a maximum LWP at 06h LST in the morning before sunrise, followed by a decrease until about 16h LST and an increase afterwards. During the night LWP continues to increase until sunrise, as indicated by the TMI night retrievals. At around 06h LST the two-year-

485 mean all-sky LWP values are ~75 g m^{-2} for both TMI and SEVIRI, but they decrease to ~40 g m^{-2} by ~14h LST. This decrease in LWP is linked to a sharp decline in COT from 11.5 to 5.5. The relative variation in CER is much smaller over most of this time period, in agreement with Zuidema and Hartmann (1995). CER increased by 2 μm in the early hours between 06h and 10h LST, stayed around 11.0-11.5 μm most of the day, and decreased by ~1 μm in the late afternoon by 18h LST. As a result, the diurnal cycle of LWP was mainly driven by COT. Note that the all-

490 sky two-year-mean TMI (red solid line circles), SEVIRI (black solid line circles), and MODIS (colored circles) LWPs exhibit excellent agreement not only in their relative diurnal variations but also in their absolute values –the curves almost completely overlap.

    For the overcast case, a ~30 % increase in COT and a slight <1 μm decrease in CER lead to an overall increase of 25–30 g m^{-2} (~40 %) in mean LWP compared to the all-sky case. Apart from that, the diurnal cycles of

495 LWP, COT, and CER are very similar between the overcast and all-sky cases. The standard SEVIRI (black dash-dot line, plus signs) and TMI day (red dash-dot line, plus signs) overcast LWPs also show very good quantitative agreement, with SEVIRI being biased high only about 5 g m^{-2}. Note that for the two-year means, adiabatic SEVIRI

LWPs (green dashed line, triangles) had larger and negative biases than standard SEVIRI retrievals. As shown later, this was the consequence of the significant smoke-induced negative biases in SEVIRI retrievals in the aerosol-

500   affected seasons of JJA and SON. In the smoke-free seasons of DJF and MAM, adiabatic SEVIRI LWPs were in better agreement with TMI microwave LWPs than were standard SEVIRI LWPs, echoing the findings of Bennartz (2007) and Seethala and Horváth (2010) for MODIS – AMSRE-E LWP comparison.

Comparing MODIS Terra (10h LST) and Aqua (14h LST) LWPs, a similar decreasing diurnal trend can be observed, except that MODIS LWPs are 5–10 g m^{-2} larger than SEVIRI LWPs for the overcast case, probably due to

505   the difference in pixel size (1 km vs. 3 km). The CM SAF (2016) validation report also suggests that the coarser resolution of SEVIRI retrievals results in somewhat lower COT and LWP values compared to MODIS, due to non-linear averaging effects (plane-parallel albedo bias).

Our results are consistent with Wood et al. (2002) and Painemal et al. (2012), who studied the diurnal variation of LWP over the southeast Atlantic and southeast Pacific Sc, based on microwave and near-infrared

510   satellite data. Similar to our results, Painemal et al. (2012) also noted that COT rather than CER explains most of the LWP variation. Blaskovic et al. (1990) associated the daytime decrease of LWP with the decrease of cloud thickness observed in their ground-based measurements, as the cloud base height increased from sunrise till mid-afternoon, while cloud top height decreased in the late afternoon. Duynkerke et al. (2004) found that the diurnal variation of Sc LWP is related to the transition from a decoupled MBL during daytime to a vertically well-mixed MBL during the

515   night. The observed diurnal cycle of Sc is characterized by a cloud layer that gradually thickens during the night but gets thinner during the day due to absorption of shortwave radiation and decoupling. The latter state exhibits slightly negative buoyancy fluxes and a minimum vertical velocity variance near cloud base. This implies that surface-driven, moist thermals cannot penetrate the cloud layer, while entrainment maintains a steady supply of relatively warm and dry air from just above the inversion into the cloud layer, resulting in a distinct LWP diurnal cycle with

520   minimum values during the day. The diurnal cycle of LWP also consistently follows the variation of cloud fraction in our data. This is in agreement with Fairall et al. (1990) and Ciesielski et al. (2001), who observed that fractional cloudiness is maximum in the predawn hours and minimum in the mid-afternoon, which is accompanied by an opposite trend in the MBL moisture with a predawn drying and an afternoon moistening.

The seasonal mean diurnal cycles of Sc clouds are qualitatively similar to the two-year mean, except for the

525   aerosol affected months of JJA (Figs. 7 and S7-S9). The maximum LWP tends to occur between 06h and 10h LST. The largest diurnal variation is seen during SON, which is also the season with the greatest cloud cover. We found

that the relative amplitude of the two-year- and seasonal-mean LWP diurnal cycle is typically 35-40 %. Wood et al. (2002) reported diurnal amplitudes of 15-35 % in MBL clouds using TMI data and Zuidema and Hartmann (1995) obtained a 25 % variation in LWP over the North/South Pacific as well as South Atlantic stratus clouds using SSM/I

530   data for the summer months. However, Fairall et al. (1990) found larger amplitudes of 60-70 % for Californian Sc clouds using a 17-day period of near-continuous ground-based microwave radiometer data.

In the all-sky case, the diurnal variation of TMI and SEVIRI LWP is in good absolute agreement within ±5 g m^{-2}, for all seasons and the two-year mean, except JJA. In JJA, however, a ±10 g m^{-2} or even slightly larger mean difference is found between the techniques, despite the exclusion of aerosol-affected pixels with AI > 0.1. MODIS

535   Terra and Aqua mean LWPs also show excellent agreement with the corresponding SEVIRI LWPs within ±5 g m^{-2}, for all seasons and the two-year mean.

In the overcast case, SEVIRI LWPs are 10–20 g m^{-2} larger than TMI LWPs especially for the aerosol-free seasons of DJF and MAM. After applying the adiabatic correction, the biases become negligible between the datasets. For the aerosol-affected seasons of JJA and SON, the mean SEVIRI LWPs likely underestimate the actual

540   values and hence applying adiabatic correction (reduction) worsens the comparison with TMI LWPs. In the overcast case, MODIS Terra and Aqua LWPs deviate by 5–10 g m^{-2} from SEVIRI LWPs for the aerosol-free seasons, but by a larger amount of 5–20 g m^{-2} for the aerosol-affected seasons due to smoke-induced biases being larger in SEVIRI than MODIS retrievals (see section 4.2).

Seasonally COT varies between 4 and 16, typically showing a relative decrease of 40–50 % from early

545   morning to late afternoon. Not surprisingly, the diurnal amplitude of COT is similar to that of LWP. Although the absolute value of CER varies from 7 to 12 μm between different seasons, the relative diurnal variation is negligible. The diurnal reduction in COT is likely due to the reduction in cloud fraction and cloud physical thickness, while the variation in cloud-top CER is probably indicative of enhanced cloud-top entrainment of dry air and associated droplet evaporation. Although MODIS COTs are slightly higher in both Aqua and Terra data, the difference with

550   SEVIRI is only about 1, while MODIS CER values are within 2 μm of the SEVIRI CER.

5. Summary

The objective of this work was to compare LWP, COT, and CER retrievals from SEVIRI, MODIS, and TMI, in order to quantify the effect of biomass burning smoke on passive VIS/NIR imager retrievals as well as to evaluate

555   the diurnal cycle of South Atlantic maritime stratocumulus clouds. In general, SEVIRI and TMI showed good

agreement for instantaneous and domain-mean LWPs in the Sc region, while the agreement in the broken cloud region was worse. Spatial distributions showed a correlation higher than 0.85 between the all-sky retrievals, with negligible bias on a two-year and seasonal basis for all smoke-free months. Boreal summer months were heavily smoke-affected and hence a larger bias was observed between the VIS/NIR and microwave techniques, due to an

560   underestimation in the former. For overcast cases, the mean LWPs were ~60 % greater than the all-sky LWPs in both SEVIRI and TMI. In biomass smoke-free months, the overcast SEVIRI LWPs were higher than the corresponding TMI LWPs; however, an adiabatic correction could reduce this high bias to the 5 % level. In smoke-affected months, in contrast, the adiabatic correction, which amounts to a ~17 % reduction in VIS/NIR LWP, further increased the (negative) bias between SEVIRI and TMI. This was so because SEVIRI retrievals were already biased

565   low by the presence of absorbing aerosols over clouds, even though aerosol index-based filtering was applied to exclude the most polluted pixels.

SEVIRI and MODIS LWPs showed excellent correlation of > 0.9 in the Sc region on a two-year and seasonal basis. However, mean MODIS COTs and CERs were 5–10 % higher in smoke-free months and 10–20 % higher in smoke-affected months than corresponding SEVIRI mean values. Interestingly, in overcast cases the

570   relative magnitudes of MODIS CER retrievals from the 1.6-, 2.1-, and 3.7-μm channels were different in smoke-free and smoke-affected months. Especially in JJA, the 1.6-μm MODIS CER was significantly lower than the other two values, indicating a strong low bias in this channel due to smoke absorption. Overall, the difference between SEVIRI and MODIS LWPs was within 5 % in smoke-free seasons, but the retrieved SEVIRI LWPs were 10–25 % lower than MODIS LWPs in smoke-affected months.

575   Prompted by the above, we separately investigated the influence of absorbing aerosols over the Sc domain using aerosol index obtained from OMI. While TMI LWP showed a steep increase with AI, SEVIRI LWP showed a systematic decrease. This indicates that absorbing aerosols above liquid clouds introduce substantial negative retrieval biases in VIS/NIR cloud optical thickness and droplet effective radius, and, hence, in the deduced LWP. This bias in SEVIRI LWP increased with AI and could be as large as 40 g m^{-2} in instantaneous retrievals. Neglecting

580   aerosol-affected pixels with AI>0.1, the domain-mean TMI minus SEVIRI LWP bias could be reduced but not completely removed. Similar to SEVIRI, all three MODIS channels showed a decrease in LWP with AI, with the largest decrease occurring in the 1.6-μm channel. The overall reduction in LWP with AI was 10–20 % in MODIS retrievals, whereas it was ~50 % in SEVIRI retrievals; the difference can partially be explained by the different non-

absorbing VIS channel used: the 0.8-μm channel used for MODIS retrievals is less affected by aerosol absorption than the 0.6-μm channel used for SEVIRI.

In the all-sky case, the diurnal variations of TMI and SEVIRI LWP were in good absolute agreement, being within ±5 g m^{-2} for all seasons and the two-year mean, except JJA. In JJA, the season most affected by biomass smoke, a larger mean difference was found between the techniques, although we eliminated aerosol-affected pixels with AI > 0.1. MODIS Terra and Aqua mean LWPs also showed excellent agreement with corresponding SEVIRI LWPs in the all-sky case, differences being within ±5 g m^{-2} for all seasons and two-year means.

In the overcast case, SEVIRI LWPs were 10–20 g m^{-2} larger than TMI LWPs especially in the smoke-free seasons of DJF and MAM. After applying an adiabatic correction to SEVIRI retrievals, however, the biases between the datasets became negligible. In the smoke-affected seasons of JJA and SON, the mean SEVIRI LWPs already underestimated the TMI values due to smoke-induced retrieval biases and hence applying the adiabatic correction (i.e. further reduction) worsened the comparison with TMI LWPs. In the overcast case, MODIS Terra and Aqua LWPs differed by 5–10 g m^{-2} from SEVIRI LWPs in smoke-free seasons and by a larger amount of 5–20 g m^{-2} in smoke-affected seasons, due to the different magnitudes of smoke-induced biases in SEVIRI and MODIS retrievals.

Irrespective of season, both TMI and SEVIRI LWP decreased from morning to mid-afternoon, and after that a slight increase was observed. Prior to sunrise clouds are the thickest and as the day progresses the cloud layer thins due to the absorption of solar radiation and associated decoupling of the sub-cloud layer. We found that the relative amplitude of the LWP diurnal cycle is typically 30-50%, which is close to but slightly larger than the diurnal amplitude reported in most previous studies. The temporal variation in SEVIRI LWP was mainly due to that in cloud optical thickness, while droplet effective radius showed relatively small diurnal variability. MODIS Terra (morning) and Aqua (afternoon) LWPs indicated a similar diurnal trend, but MODIS LWPs were 5–10 g m^{-2} larger than SEVIRI/TMI values in the overcast case. This maybe partly due to the plane-parallel albedo bias affecting the larger SEVIRI pixels.

While the discrepancies between microwave and VIS/NIR LWP retrievals in areas of broken clouds with low cloud fraction require further research to be fully resolved, our study has shown that there is a reasonable consensus between the techniques about the seasonal and diurnal cycles of LWP in nearly overcast stratocumulus fields. This lends some credibility to the VIS/NIR retrievals of the underlying cloud microphysical properties. In our opinion, SEVIRI-derived CLAAS-2 cloud property observations provide a useful resource for the evaluation of stratocumulus cloud diurnal cycles in climate models.

615 **Acknowledgements**

The work of the first author was funded by EUMETSAT through the CM SAF Visiting Scientist scheme and was done at the Royal Netherlands Meteorological Institute, De Bilt, Netherlands. SEVIRI CLAAS-2 CPP retrievals were obtained from https://doi.org/10.5676/EUM_SAF_CM/CLAAS/V002. TMI data were produced by Remote Sensing Systems and sponsored by the NASA Earth Sciences Program. Data are available at
620 www.remss.com/missions/tmi. OMI data were downloaded from http://mirador.gsfc.nasa.gov/ and Aqua/Terra MODIS Level-2 data were obtained from http://ladsweb.nascom.nasa.gov/.

625

630

635

640

References

Abel, S. J., Walters, D. N., and Allen, G.: Evaluation of stratocumulus cloud prediction in the Met Office forecast model during VOCALS-REx, Atmos. Chem. Phys., 10, 10541-10559, doi:10.5194/acp-10-10541-2010, 2010.

645 Adebiyi, A. A. and Zuidema, P.: The role of the southern African easterly jet in modifying the southeast Atlantic aerosol and cloud environments, Quart. J. Roy. Met. Soc., 142:697, 1574-1589, https://doi.org/10.1002/qj.2765, 2016.

Adebiyi, A. A., Zuidema, P., and Abel, S. J.: The Convolution of Dynamics and Moisture with the Presence of Shortwave Absorbing Aerosols over the Southeast Atlantic, J. Climate, Volume 28, pg.1997-2024, doi: 650 10.1175/JCLI-D-14-00352.1, 2015.

Albrecht, B.A., Jensen, M. P., and Syrett, W. J.: Marine boundary layer structure and fractional cloudiness, J. Geophys. Res., 100 (D7), 14209-14222, https://doi.org/10.1029/95JD00827, 1995.

Benas, N., Finkensieper, S., Stengel, M., van Zadelhoff, G.J., Hanschmann, T., Hollmann, R., and Meirink, J. F.: The MSG-SEVIRI-based cloud property data record CLAAS-2, Earth Syst. Sci. Data, 9, 415-434, 655 https://doi.org/10.5194/essd-9-415-2017, 2017.

Bennartz, R.: Global assessment of marine boundary layer cloud droplet number concentration from satellite, J. Geophys. Res., 112, D02201, doi:10.1029/2006JD007547, 2007.

Bennartz, R. and Harshvardhan: Correction to "Global assessment of marine boundary layer cloud droplet number concentration from satellite", J. Geophys. Res., 112, D16302, doi:10.1029/2007JD008841, 2007.

660 Bennartz, R., and Rausch, J.: Global and regional estimates of warm cloud droplet number concentration based on 13 years of AQUA-MODIS observations. Atmos. Chem. Phys., doi:10.5194/acp-17-9815-2017, 2017

Betts, A. K.: The diurnal variation of California coastal stratocumulus from two days of boundary layer soundings, Tellus, 42A, 302–304, https://doi.org/10.3402/tellusa.v42i2.11879, 1990.

Blaskovic, M., Davies, R., and Snider, J. B.: Diurnal variation of marine stratocumulus over San Nicolas island 665 during July, 1987, C2GGR Report No. 90-6, https://doi.org/10.1175/1520-0493, 1990.

Bony, S., and Dufresne, J. L.: Marine boundary layer clouds at the heart of tropical cloud feedback uncertainties in climate models, Geophys. Res. Lett., 32, L20806, doi:10.1029/2005GL023851, 2005.

Borg, L. A., and Bennartz, R.: Vertical structure of stratiform marine boundary layer clouds and its impact on cloud albedo, Geophys. Res. Lett., 34, L05807, doi:10.1029/2006GL028713, 2007.

670   Bretherton, C. S., and Wyant, W. C.: Moisture transport, lower-tropospheric stability, and decoupling of cloud-topped boundary layers, J. Atmos. Sci., 54, 148–167, https://doi.org/10.1175/1520-0469, 1997.

Bretherton, C. S., Austin, P. H., and Siems, S. T.: Cloudiness and Marine Boundary Layer Dynamics in the ASTEX Lagrangian Experiments. Part II: Cloudiness, Drizzle, Surface Fluxes and Entrainment, J. Atmos. Sci., 52, 2724–2735, https://doi.org/10.1175/1520-0469, 1995.

675   Burleyson, C. D., De Szoeke, S. P., Yuter, S. E., Wilbanks, M., and Brewer, W. A.: Ship-Based Observations of the Diurnal Cycle of Southeast Pacific Marine Stratocumulus Clouds and Precipitation, J. Atmos. Sci., 70, 3876–3894, https://doi.org/10.1175/JAS-D-13-01.1, 2013.

Chang, I. and Christopher, S. A.: The impact of seasonalities on direct radiative effects and radiative heating rates of absorbing aerosols above clouds, Quart. J. Roy. Met. Soc., 143:704, 1395-1405,

680   https://doi.org/10.1002/qj.3012, 2017.

Cho, H. M., Zhang, Z., Meyer, K., Lebsock, M., Platnick, S., Ackerman, A. S., Di Girolamo, L., Labonnote, L., Cornet, C., Riedi, J., and Holz, R.: Frequency and causes of failed MODIS cloud property retrievals for liquid phase clouds over global oceans: Failed MODIS Cloud Retrievals. J. Geophys. Res.: Atmospheres, 120, Doi:10.1002/2015JD023161, 2015.

685   Ciesielski, P. E., Schubert, W. H., and Johnson, R. H.: Diurnal Variability of the Marine Boundary Layer during ASTEX, J. Atmos. Sci., 58, 2355-2376, https://doi.org/10.1175/1520-0469, 2001.

CM SAF: Algorithm Theoretical Basis Document, SEVIRI Cloud Physical Products, CLAAS Edition 2, EUMETSAT Satellite Application Facility on Climate Monitoring, SAF/CM/KNMI/ATBD/SEVIRI/CPP, Issue 2, Rev. 2, https://doi.org/10.5676/EUM_SAF_CM/CLAAS/V002, 10 June 2016b.

690   Coddington, O. M., Pilewskie, P., Redemann, J., Platnick, S., Russell, P. B., Schmidt, K. S., Gore, W. J., Livingston, J., Wind, G., and Vukicevic, T.: Examining the impact of overlying aerosols on the retrieval of cloud optical properties from passive remote sensing, J. Geophys. Res., 115, D10211, doi:10.1029/2009JD012829, 2010.

Duynkerke, P. G., De Roode, S. R., Van Zanthen, M. C., Calvo, J., Cuxart, J., Cheinet, S., Chlond, A., Grenier, H., Jonker, P. J., Köhler, M., Lenderink, G., Lewellen, D., Lappen, C., Lock, A. P., Moeng, C. Müller, F., Olmed,

695   D., Piriou, J., Sanchez, E., and Sednev, I.: Observations and numerical simulations of the diurnal cycle of the EUROCS stratocumulus case, Quart. J. Roy. Met. Soc., 130, 3269-3296, doi: 10.1256/qj.03.139, 2004.

Eastman, R., Warren, S. G., and Hahn, C. J.: Variations in cloud cover and cloud types over the ocean from surface observations, 1954–2008, J. Climate, 24, 5914–5934, https://doi.org/10.1175/2011JCLI3972.1, 2011.

Elsaesser, G.S., O'Dell, C. W., Lebsock, M. D., Bennartz, R., Greenwald, T. J., and Wentz, F. J.: The Multisensor

700   Advanced Climatology of Liquid Water Path (MAC-LWP), J. Climate, **3**0, 10193–10210,

https://doi.org/10.1175/JCLI-D-16-0902.1, 2017.

Fairall, C.W., Hare, J. E., and Snider, J. B.: An eight-month of marine stratocumulus cloud fraction, albedo, and

integrated liquid water, J. Climate, 3, 847-864, https://doi.org/10.1175/1520-0442, 1990.

Forster, P., et al.: Changes in atmospheric constituents and in radiative forcing, in Climate Change 2007: The

705   Physical Science Basis. Contribution of Working Group I to the Fourth Assessment Report of the

Intergovernmental Panel on Climate Change, edited by S. Solomon et al., pp. 130–234, Cambridge Univ.

Press, New York, 2007.

Greenwald T. J.: A 2 year comparison of AMSR-E and MODIS cloud liquid water path observations, Geophys Res

Lett., 36, L20805, https://doi.org/10.1029/2009GL040394, 2009.

710   Greenwald, T. J., L'Ecuyer, T. S., and Christopher, S. A.: Evaluating specific error characteristics of microwave-

derived cloud liquid water products, Geophys. Res. Lett., 34, L22807, doi:10.1029/2007GL031180, 2007.

Greenwald, T. J., Bennartz, R., Lebsock, M., & Teixeira, J.: An Uncertainty Data Set for Passive Microwave

Satellite Observations of Warm Cloud Liquid Water Path. Journal of Geophysical Research: Atmospheres,

123, 3668–3687, https://doi.org/10.1002/2017JD027638, 2018.

715   Greuell, W., Van Meijgaard, E., Meirink, J. F., and Clerbaux, N.: Evaluation of model predicted top-of-atmosphere

radiation and cloud parameters over Africa with observations from GERB and SEVIRI, J. Climate, 24,

4015-4036, doi:10.1175/2011JCLI3856.1, 2011.

Grosvenor, D. P., Sourdeval, O., Zuidema, P., et al.: Remote sensing of droplet number concentration in warm

clouds: A review of the current state of knowledge and perspectives, Doi:10.1029/2017rg000593, 2018.

720   Han Q, Rossow, W. B., and Lasis, A. A.: Near-Global Survey of Effective Droplet Radii in Liquid Water Clouds

Using ISCCP Data, J. Climate 7, 465-497, https://doi.org/10.1175/1520-0442, 1994.

Haywood, J. M., Osborne, S. R., and Abel, S. J.: The effect of overlying absorbing aerosol layers on remote sensing

retrievals of cloud effective radius and cloud optical depth, Quart. J. Roy. Met. Soc., 130, 779-800, doi:

10.1256/qj.03.100, 2004.

725   Hilburn, K., and Wentz, F. J.: Intercalibrated passive microwave rain products from the unified microwave ocean

retrieval algorithm (UMORA), J. Appl. Met. Clim., 47, 778–794,

https://doi.org/10.1175/2007JAMC1635.1, 2008.

Hobbs, P. V.: Clean air slots amid atmospheric pollution, Nature, 415, 861, doi:10.1038/415861a, 2002.

Horowitz, H. M., Garland, R. M., Thatcher, M., Landman, W. A., Dedekind, Z., Van der Merwe, J.,
730   and Engelbrecht, F. A.: Evaluation of climate model aerosol seasonal and spatial variability over Africa using
        AERONET, *Atmos. Chem. Phys.,* 17:22, 13999-14023, https://doi.org/10.5194/acp-17-13999-2017, 2017.

Horváth, Á., and Gentemann, C.: Cloud-fraction-dependent bias in satellite liquid water path retrievals of shallow,
        non-precipitating marine clouds, Geophys. Res. Lett., 34, L22806, doi:10.1029/2007GL030625, 2007.

Horváth, Á., and Davies, R.: Comparison of microwave and optical cloud water path estimates from TMI, MODIS,
735   and MISR, J. Geophys. Res., 112, D01202, doi:10.1029/2006JD007101, 2007.

Horváth, Á., Seethala, C., and Deneke, H.: View angle dependence of AMSR-E and MODIS cloud liquid water path
        retrievals in warm oceanic clouds, J. Geophys. Res., 119, 8304–8328, doi:10.1002/2013JD021355, 2014.

James, D. G.: Observations from aircraft of temperatures and humidities near stratocumulus clouds, Quart. J. Roy.
        Met. Soc., 85, 120-130, https://doi.org/10.1002/qj.49708536405, 1959.

740   Johnson, B. T., Shine, K. P., Forster, P. M.: The semi-direct aerosol effect: Impact of absorbing aerosols on marine
        stratocumulus, Quart. J. Roy. Met. Soc., 130, 1407-1422, https://doi.org/10.1256/qj.03.61, 2004.

Kar, J., Vaughan, M., Tackett, J., Liu, Z., Omar, A., Rodier, S., Trepte, C., and Lucker, P.: Swelling of transported
        smoke from savanna fires over the Southeast Atlantic Ocean, *Rem. Sen. Env.,* 211, 105-111,
        https://doi.org/10.1016/j.rse.2018.03.043, 2018.

745   Klein S. A., and Hartmann, D. L.: The seasonal cycle of low stratiform clouds, J. Climate, 6, 1587-1606,
        https://doi.org/10.1175/1520-0442-1993,1993.

Klein, S. A., Hartmann, D. L., and Norris, J.: On the Relationships among Low-Cloud Structure, Sea Surface
        Temperature, and Atmospheric circulation in the Summer time Northeast Pacific, J. Climate, 8, 1140–1155,
        https://doi.org/10.1175/1520-0442-1995, 1995.

750   Kniffka, A., Stengel, M., Lockhoff, M., Bennartz, R., and Hollmann, R.: Characteristics of cloud liquid water path
        from SEVIRI onboard the Meteosat Second Generation 2 satellite for several cloud types, Atmos. Meas.
        Tech., 7, 887-905, doi:10.5194/amt-7-887-2014, 2014.

Liu, Z., Liu, X., Zhang, Z., Zhao, C., Meyer, K., Rajapakshe, C., Wu, C., Yang, Z., and Penner, J. E.: (2018)
        Biomass smoke from southern Africa can significantly enhance the brightness of stratocumulus over the
755   southeastern Atlantic Ocean, *Pro. Nat. Acad. Sci.,* 115:12, 2924-2929,
        https://doi.org/10.1073/pnas.1713703115, 2018.

McGill, M. J., Hlavka, D. L., Hart, W. D., Welton, E. J., and Campbell, J. R.: Airborne lidar measurements of aerosol optical properties during SAFARI-2000, J. Geophys. Res., 108, 8493, doi:10.1029/2002JD002370, 2003.

760   Medeiros, B., and Stevens, B.: Revealing differences in GCM representations of low clouds, Clim. Dyn., 36, 385-399, doi:10.1007/s00382-009-0694-5, 2011.

Medeiros, B., Williamson, D. L., Hannay, C., and Olson, J. G.: Southeast Pacific stratocumulus in the Community Atmosphere Model, J. Climate, 25, 6175-6192, https://doi.org/10.1175/JCLI-D-11-00503.1, 2012.

Meehl, G. A., Covey, C., Delworth, T., Latif, M., McAvaney, B., Mitchell, J. F. B., Stouffer, R. J., and Taylor, K.

765   E.: The WCRP CMIP3 multi-model dataset: A new era in climate change research, Bull. Amer. Met. Soc., 88, 1383-1394, https://doi.org/10.1175/BAMS-88-9-1383, 2007.

Meirink, J. F., Roebeling, R. A., and Stammes, P.: Inter-calibration of polar imager solar channels using SEVIRI, Atm. Meas. Tech., 6, 2495-2508, doi:10.5194/amt-6-2495-2013, 2013.

Miller, R. L.: Tropical thermostats and low cloud cover. J. Climate, 10, 409-440, https://doi.org/10.1175/1520-

770   0442(1997), 1997.

Minnis, P., and Harrison, E. F.: Diurnal variability of regional cloud and clear-sky radiative parameters derived from GOES data. Part I: Analysis method, J. Climate, 23, 993-1011, https://doi.org/10.1175/1520-0450(1984), 1984.

Minnis, P., Heck, P., Young, D., Fairall, C., and Snider, J.: Stratocumulus cloud properties derived from

775   simultaneous satellite and island-based instrumentation during fire, J. Appl. Met., 31, 317-339, https://doi.org/10.1175/1520-0450(1992), 1992.

Moeng, C. H., Shen, S., and Randall, D. A.: Physical processes within the nocturnal stratus-topped boundary layer, J. Atmos. Sci., 49, 2384-2401, https://doi.org/10.1175/1520-0469(1992), 1992.

Nakajima T. Y., Nakajima, T.: Determination of Cloud Microphysical Properties from NOAA-17 Measurements for

780   FIRE and ASTEX regions, J. Atmos. Sci., 52, 4043-4059, https://doi.org/10.1175/1520-0469(1995), 1995.

Nakajima, T., and King, M. D.: Determination of the optical thickness and effective particle radius of clouds from reflected solar radiation measurements, I, Theory, J. Atmos. Sci., 47, 1878-1893, https://doi.org/10.1175/1520-0469(1990), 1990.

Nicholls, S.: The dynamics of stratocumulus: Aircraft observations and comparisons with a mixed layer model,

785   Quart. J. Roy. Meteor. Soc., 110, 783–820, https://doi.org/10.1002/qj.49711046603, 1984.

Norris, J. R.: Low cloud type over the ocean from surface observations. Part I: Relationship to surface meteorology and the vertical distribution of temperature and moisture, J. Climate, 11, 369-382, https://doi.org/10.1175/1520-0442(1998), 1998.

O'Dell, C. W., Wentz, F. J., and Bennartz, R.: Cloud liquid water path from satellite-based passive microwave
790   observations: A new climatology over the global oceans, J. Climate, 21, 1721-1739, https://doi.org/10.1175/2007JCLI1958.1, 2008.

Painemal, D.: Entrainment rate diurnal cycle in marine stratiform clouds estimated from geostationary satellite retrievals and a meteorological forecast model, Geophys. Res. Lett., Doi: 10.1002/2017GL074481, 2017.

Painemal, D., Kato, S, and Minnis, P.: Boundary layer regulation in the southeast Atlantic cloud microphysics
795   during the biomass burning season as seen by the A-train satellite constellation, J. Geophys. Res. Atmos., 119, 11,288–11,302, doi:10.1002/2014JD022182, 2014.

Painemal, D., Minnis, P., Ayers, J. K., and O'Neill, L.: GOES-10 microphysical retrievals in marine warm clouds: Multi-instrument validation and daytime cycle over the southeast Pacific, J. Geophys. Res., 117, D19212, doi:10.1029/2012JD017822, 2012.

800   Platnick, S.: Vertical photon transport in cloud remote sensing problems, J. Geophys. Res., 105, 22,919-22,935, https://doi.org/10.1029/2000JD900333, 2000.

Platnick, S., Meyer, K. G., King. M. D., Wind, G., Amarasinghe, N., Marchant, B., Arnold, G. T., Zhang, Z., Hubanks, P. A., Holz, R. E., Yang, P., Ridgway, W. L., and Riedi, J.: The MODIS Cloud Optical and Microphysical Products: Collection 6 Updates and Examples From Terra and Aqua, IEEE T. Geosci. Remote,
805   55, 502–525, https://doi.org/10.1109/TGRS.2016.2610522, 2017.

Rahn, D., and Garreaud, R.: Marine boundary layer over the subtropical southeast Pacific during VOCALS-REx - Part 1: Mean structure and diurnal cycle, Atmos. Chem. Phys., 10, 4491-4506, doi:10.5194/acp-10-4491-2010, 2010.

Rajapakshe, C., Zhang, Z., Yorks, J., Yu, H., Tan, Q., Meyer, K., Platnick, S., Winker, D. M.: Seasonally
810   Transported Aerosol Layers over Southeast Atlantic are Closer to Underlying Clouds than Previously Reported, Geophys. Res. Lett., 44, Doi:10.1002/2017GL073559, 2017.

Rausch, J., Meyer, K., Bennartz, R., and Platnick, S.: Differences in liquid cloud droplet effective radius and number concentration estimates between MODIS collections 5.1 and 6 over global oceans, Atmos. Meas. Tech., 10, 2105–2116, https://doi.org/10.5194/amt-10-2105-2017, 2017.

815

Randles, C. A. and Ramaswamy, V.: Direct and semi-direct impacts of absorbing biomass burning aerosol on the climate of southern Africa: a Geophysical Fluid Dynamics Laboratory GCM sensitivity study, Atmos. Chem. Phys., 10, 9819-9831, doi:10.5194/acp-10-9819-2010, 2010.

Roebeling, R. A., Feijt, A. J., and Stammes, P.: Cloud property retrievals for climate monitoring: Implications of
820   differences between Spinning Enhanced Visible and Infrared Imager (SEVIRI) on METEOSAT-8 and Advanced Very High Resolution Radiometer (AVHRR) on NOAA-17, J. Geophys. Res., 111D20210 10.1029/2005jd006990, 2006.

Roebeling, R. A., and E. Van Meijgaard, E.: Evaluation of the Daylight Cycle of Model-Predicted Cloud Amount and Condensed Water Path over Europe with Observations from MSG SEVIRI, J. Climate, 22, 1749-
825   176610.1175/2008jcli2391.1, 2009.

Rozendaal M. A., Leovy, C. B., and Klein, S. A.: An observational study of diurnal variations of marine stratiform cloud, J. Climate, 8, 1795-1809, https://doi.org/10.1175/1520-0442(1995), 1995.

Sandu, I., Stevens, B., and Pincus, R.: On the transitions in marine boundary layer cloudiness, Atmos. Chem. Phys., 10, 2377-2391, https://doi.org/10.5194/acp-10-2377-2010, 2010.

830   Schulz, J., Albert, P., Behr, H. D., Caprion, D., Deneke, H., Dewitte, S., Durr, B., Fuchs, P., Gratzki, A., Hechler, P., Hollmann, R., Johnston, S., Karlsson, K. G., Manninen, T., Muller, R., Reuter, M., Riihela, A., Roebeling, R., Selbach, N., Tetzlaff, A., Thomas, W., Werscheck, M., Wolters, E., and Zelenka, A.: Operational climate monitoring from space: the EUMETSAT Satellite Application Facility on Climate Monitoring (CM SAF), Atmos. Chem. Phys., 9, 1687-1709, https://doi.org/10.5194/acp-9-1687-2009, 2009.

835   Seethala, C., and. Horváth, Á.: Global assessment of AMSR-E and MODIS cloud liquid water path retrievals in warm oceanic clouds, J. Geophys. Res., 115, D13202, doi:10.1029/2009JD012662, 2010.

Stephens G. L., Paltridge, G. W., and Platt, C. M. R.: Radiation profiles in extended water clouds. III. Observations. J. Atmos. Sci., 35, 2133-2141, https://doi.org/10.1175/1520-0469(1978), 1978.

Torres, O., Tanskanen, A., Veihelmann, B., Ahn, C., Braak, R., Bhartia, P. K., Veefkind, P., and Levelt, P.: Aerosols
840   and surface UV products from Ozone Monitoring Instrument observations: An overview, J. Geophys. Res., 112, D24S47, doi:10.1029/2007JD008809, 2007.

Watts P. D., Mutlow C. T., Baran A. J., and Zavody A. M.: "Study on Cloud Properties derived from Meteosat Second Generation Observations," Final Report, EUMETSAT ITT no. 97/181, 1998.

Wentz, F. J.: A 17-Yr Climate Record of Environmental Parameters Derived from the Tropical Rainfall Measuring

845   Mission (TRMM) Microwave Imager, J. Climate, 28, 6882-6902, https://doi.org/10.1175/JCLI-D-15-0155.1,

2015.

Wentz, F. J, and Spencer, R.: SSM/I rain retrievals within a unified all-weather ocean algorithm, J. Atmos. Sci., 55,

1613-1627, https://doi.org/10.1175/1520-0469(1998), 1998.

Wentz, F. J.: A well-calibrated ocean algorithm for special sensor microwave/imager, J. Geophys. Res., 102, 8703-

850   8718, https://doi.org/10.1029/96JC01751, 1997.

Wilcox, E. M., Harshvardhan, and Platnick, S.: Estimate of the impact of absorbing aerosol over cloud on the

MODIS retrievals of cloud optical thickness and effective radius using two independent retrievals of liquid

water path, J. Geophys. Res., 114, D05210, doi:10.1029/2008JD010589, 2009.

Wilcox, E. M.: Stratocumulus cloud thickening beneath layers of absorbing smoke, Aerosol, Atmos. Chem. Phys.,

855   10, 11769-11777, https://doi.org/10.5194/acp-10-11769-2010, 2010.

Wilson, C. A., and Mitchell, J. F. B.: Diurnal variation and cloud in a general circulation model, Quart. J. Roy. Met.

Soc., 112, 347-369, https://doi.org/10.1002/qj.49711247205, 1986.

Wood, R.: Stratocumulus Clouds, Monthly Weather Review, 140(8), 2373–2423, doi:10.1175/MWR-D-11-00121.1,

2012.

860 Wood, R., and Bretherton, C. S.: On the relationship between stratiform low cloud cover and lower-tropospheric

stability, J. Climate, 19, 6425–6432, https://doi.org/10.1175/JCLI3988.1, 2006.

Wood, R., Bretherton, C. S., and Hartmann, D. L.: Diurnal cycle of liquid water path over the subtropical and

tropical oceans, Geophys. Res. Lett., 29 (23), 2092, doi:10.1029/2002GL015371, 2002.

Wood, R., and Hartmann, D. L.: Spatial Variability of Liquid Water Path in Marine Low Cloud: The Importance of

865   Mesoscale Cellular Convection, J. Climate, 19, 1748-1764, https://doi.org/10.1175/JCLI3702.1, 2006.

Zelinka, M. D., Randall, D. A., Webb, M. J., and Klein, S. A.: Clearing clouds of uncertainty, Nature Climate

Change 7, 674-678, 10.1038/nclimate3402, 2017.

Zhang, Z., Ackerman, A. S., Feingold, G., Platnick, S., Pincus, R., and Xue, H.: Effects of cloud horizontal

inhomogeneity and drizzle on remote sensing of cloud droplet effective radius: Case studies based on large-

870   eddy simulations, J. Geophys. Res. Atmos., 117, D19208, https://doi.org/10.1029/2012jd017655, 2012.

Zhang, Z. and Platnick, S.: An assessment of differences between cloud effective particle radius retrievals for marine water clouds from three MODIS spectral bands, J. Geophys. Res., 116, D20215, https://doi.org/10.1029/2011jd016216, 2011.

875 Zuidema P., and Hartmann, D. L.: Satellite determination of stratus cloud microphysical properties, J. Climate, 8, 1638-1657, https://doi.org/10.1175/1520-0442(1995), 1995.

Zuidema, P., Redemann, J., Haywood, J., Wood, R., Piketh, S., Hipondoka, M., and Formenti, P.: Smoke and clouds above the southeast Atlantic: Upcoming field campaigns probe absorbing aerosol's impact on climate, Bull. Am. Met. Soc., 97: 1131–1135, https://doi.org/10.1175/BAMS-D15-00082.1, 2016.

880

885

TABLES

Table 1. Two-year mean and seasonal statistics of collocated SEVIRI and TMI LWP retrievals for rain-free, ice-free, smoke-free (AI<0.1), COT > 3, and overcast (LCF ≥ 95%) grid cells over the marine stratocumulus region. LWP means, biases (SEVIRI-TMI), and Root Mean Square Differences (RMSD) are given in g m^{-2}. COT means and CER means (in micron) are also tabulated. The values in brackets are statistics without filtering for LCF≥ 95% and COT >3, i.e., for the all-sky case. "adb" refers

890 to the overcast LWP calculation assuming adiabatic clouds.

	JJA	SON	DJF	MAM	Two-year
			Stratocumulus (SEVIRI vs. TMI)		
SEVIRI LWP	73 (48)	87 (63)	92 (52)	83 (41)	84 (53)
SEVIRI LWP adb	61	72	76	69	70
TMI LWP	82 (57)	82 (62)	76 (45)	73 (39)	80 (53)
SEVIRI-TMI LWP	-9 (-9)	5 (1)	16 (7)	10 (2)	4 (0)
SEV adb -TMI LWP	-21	-10	0	-4	-10
RMSD	31 (26)	28 (26)	22 (21)	21 (20)	28 (24)
#Samples	1.6E+5 (3.2E+5)	3.3E+5 (5.2E+5)	1.4E+5 (3.2E+5)	9.1E+4 (2.6E+5)	7.3E+5 (1.4E+6)
Correlation	0.81 (0.87)	0.86 (0.89)	0.92 (0.93)	0.93 (0.92)	0.86 (0.89)
SEVIRI COT	10.2 (6.8)	11.0 (8.2)	10.7 (6.6)	10.3 (5.7)	10.7 (7.0)
SEVIRI CER	9.4 (10.8)	10.6 (11.2)	11.6 (11.7)	10.8 (11.0)	10.6 (11.2)

895

900

905

Table 2. Two-year mean and seasonal statistics of collocated SEVIRI and MODIS retrievals in rain-free, ice-free, smoke-free (AI<0.1), COT > 3, and overcast (LCF ≥95%) grid cells over the marine stratocumulus region. LWP means, biases (MODIS-SEVIRI), and Root Mean Square Differences (RMSD) are given in g m^{-2}. Corresponding COT means and CER means are tabulated in Table S1. The values in brackets are statistics without filtering for LCF≥ 95% and COT >3, i.e., for the all-sky case. "S" and "M" refer SEVIRI and MODIS.

	JJA	SON	DJF	MAM	Two-year
Stratocumulus (SEVIRI vs. MODIS)					
SEVIRI LWP	71 (44)	81 (58)	88 (45)	81 (39)	80 (48)
MODIS 1.6 LWP	79 (46)	86 (59)	88 (45)	84 (41)	84 (49)
MODIS 2.1 LWP	85 (48)	90 (60)	89 (44)	85 (40)	88 (50)
MODIS 3.7 LWP	88 (51)	89 (59)	84 (42)	82 (38)	87 (49)
M 1.6 – S LWP	8 (2)	5 (1)	0 (0)	3 (2)	4 (1)
M 2.1 – S LWP	14 (4)	9 (2)	1 (-1)	4 (1)	8 (2)
M 3.7 – S LWP	17 (7)	8 (1)	-4 (-3)	1 (-1)	7 (1)
RMSD 1.6	17 (21)	16 (20)	17 (18)	16 (18)	17 (19)
RMSD 2.1	16 (21)	15 (19)	17 (18)	16 (19)	16 (19)
RMSD 3.7	19 (20)	19 (20)	18 (19)	18 (17)	20 (19)
#Samples	3.7E+5 (9.6E+5)	6.4E+5 (1.4E+6)	2.4E+5 (8.2E+5)	2.0E+5 (7.8E+5)	1.5E+6 (4.0E+6)
Corr. LWP 1.6	0.95 (0.91)	0.95 (0.93)	0.95 (0.94)	0.96 (0.94)	0.95 (0.93)
Corr. LWP 2.1	0.95 (0.91)	0.95 (0.93)	0.95 (0.94)	0.96 (0.93)	0.95 (0.93)
Corr. LWP 3.7	0.94 (0.92)	0.93 (0.92)	0.94 (0.93)	0.95 (0.95)	0.93 (0.93)
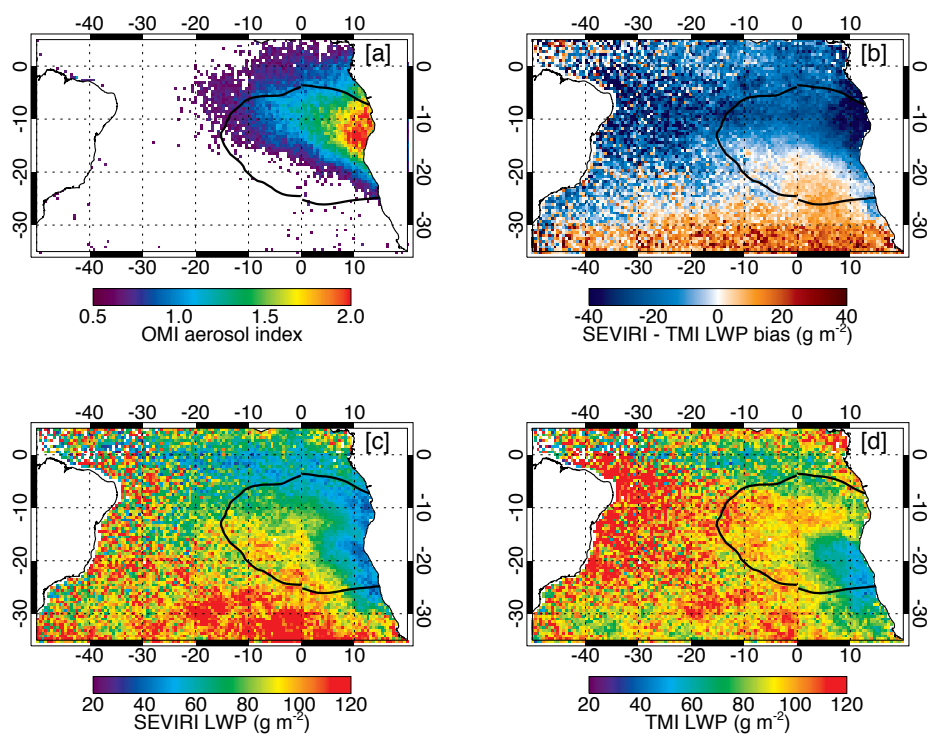
FIGURES

925

930

Figure 1. Spatial distribution of (a) OMI ultraviolet aerosol index, (b) SEVIRI minus TMI liquid water path bias, (c) SEVIRI liquid water path, and (d) TMI liquid water path, averaged for JAS in 2011 and 2012 for overcast (LCF ≥ 95% and COT > 3) rain- and ice-free conditions. The black contour denotes the identified stratocumulus region.

935
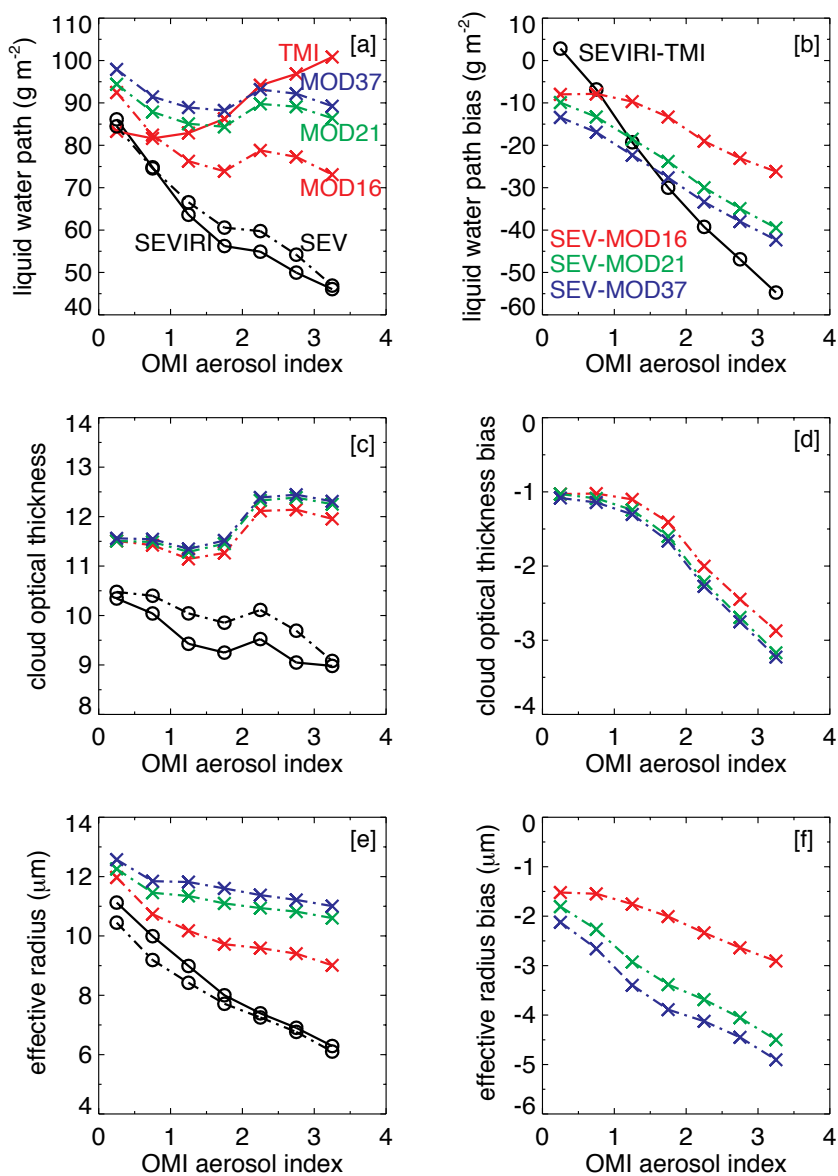
Figure 2. OMI aerosol index *versus* (a) SEVIRI, TMI and MODIS LWPs, (b) SEVIRI LWP biases compared to TMI and MODIS, (c) SEVIRI and MODIS COTs, (d) SEVIRI – MODIS COT biases, (e) SEVIRI and MODIS CER, and (f) SEVIRI –

940   MODIS CER biases, over the overcast Sc region for JAS 2011 and JAS 2012 for rain- and ice-free conditions. Solid lines correspond to SEVIRI vs. TMI comparison, whereas dash-dotted lines correspond to SEVIRI vs. MODIS comparison. The label "SEV" refers SEVIRI values at MODIS collocations.
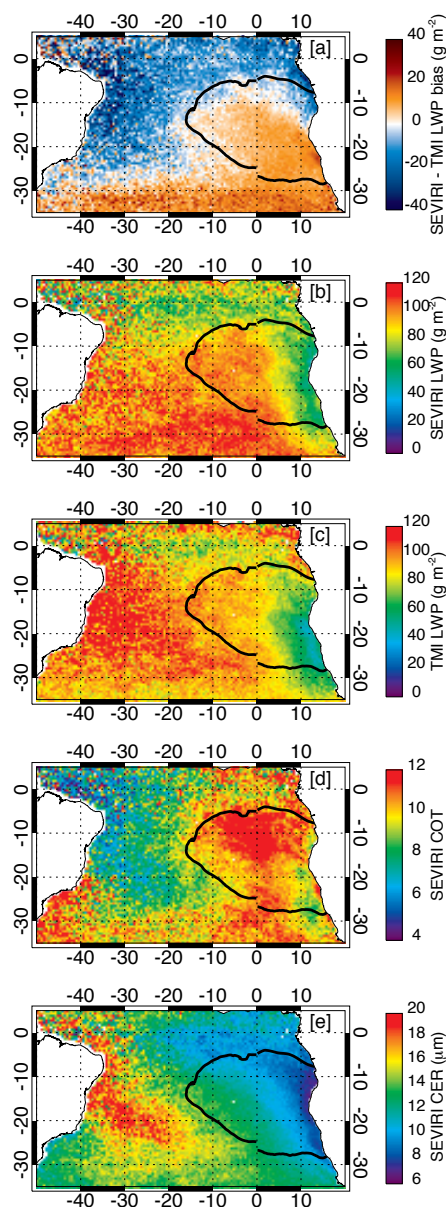
945

Figure 3. Two-year mean map of (a) SEVIRI minus TMI LWP bias, (b) SEVIRI LWP, (c) TMI LWP, (d) SEVIRI COT, (e) SEVIRI 1.6-μm CER, for the overcast case (LCF ≥ 95% and COT > 3). The solid black contour denotes the identified Sc region. Rain-, ice-, and smoke-free conditions were applied.

950

955
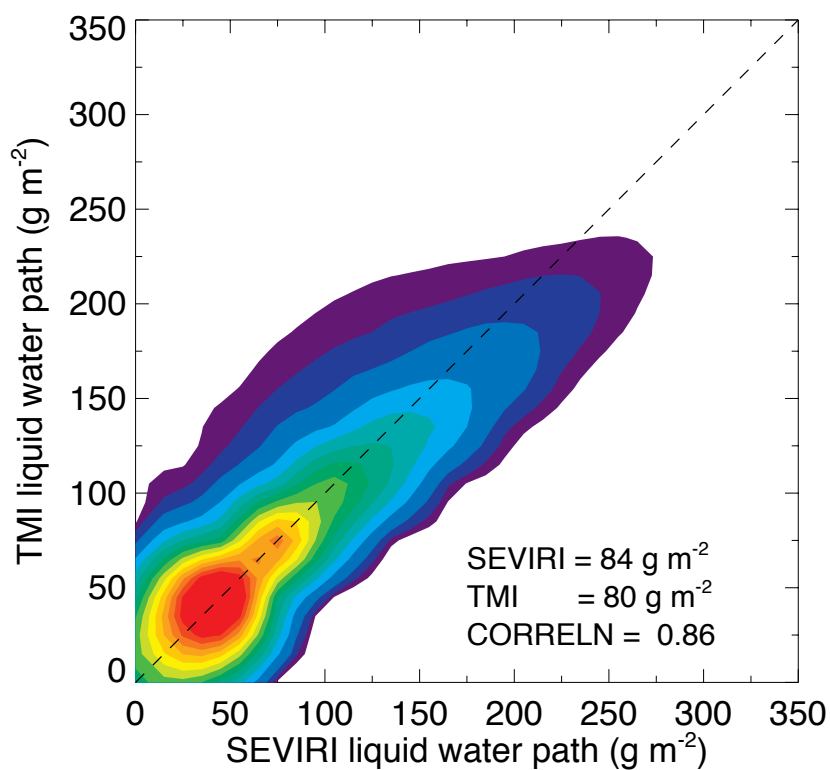
Figure 4. Scatter density plot of SEVIRI versus TMI liquid water path for the overcast case (LCF ≥ 95% and COT > 3) in two
years of data. Rain-, ice-, and smoke-free conditions were applied.

960
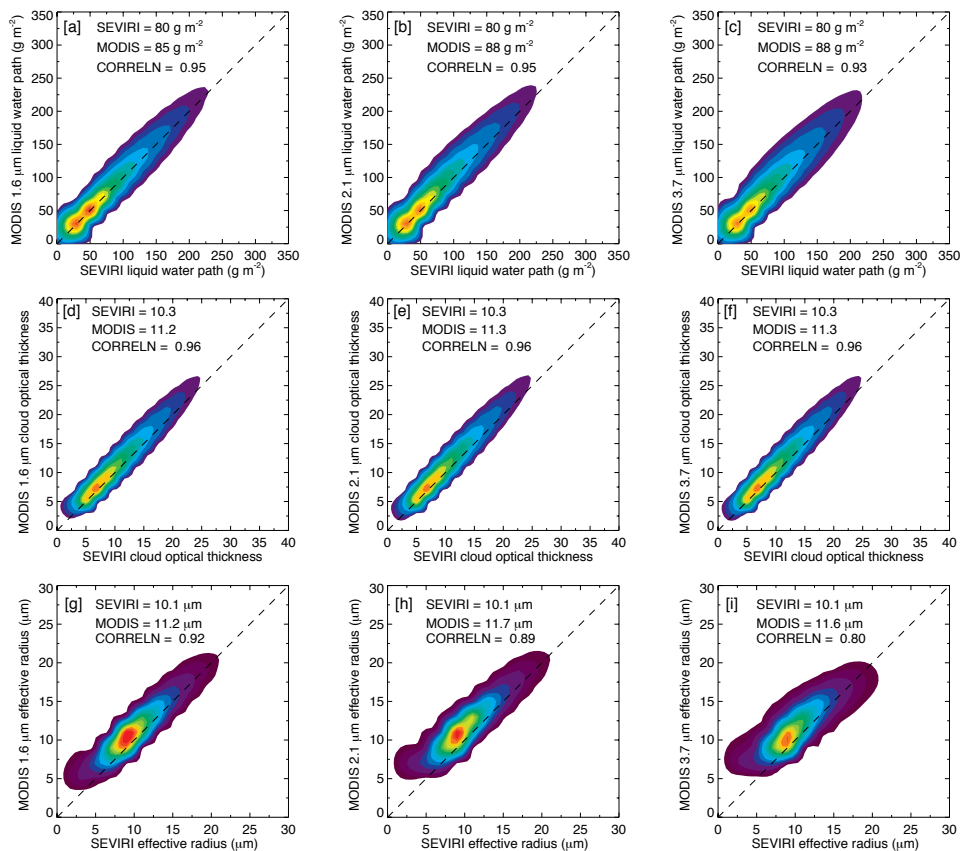
965

970

Figure 5. Scatter density plot of SEVIRI versus MODIS liquid water path, cloud optical thickness, effective radius in the overcast case (LCF ≥ 95% and COT > 3) in two years of data. Rain-, ice-, and smoke-free conditions were applied.

975

980
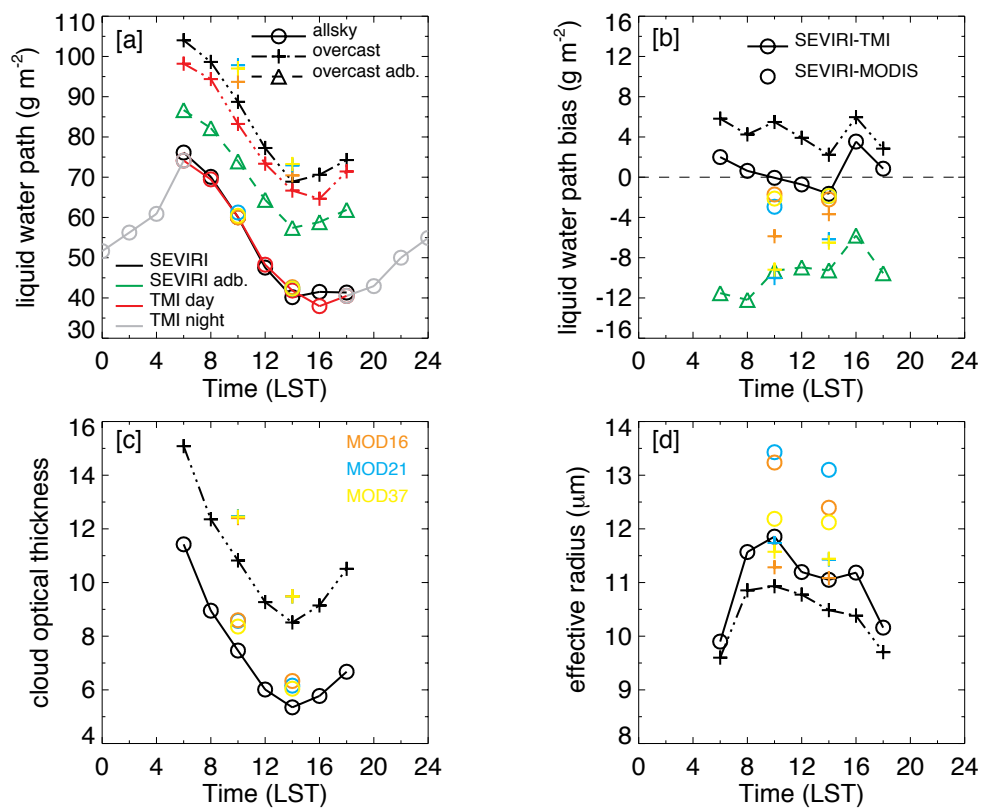
Figure 6. Two-year mean diurnal cycle of cloud properties over the Sc region, both for all-sky and overcast (LCF ≥ 95% and

985   COT > 3) cases: (a) SEVIRI and TMI LWPs, (b) SEVIRI minus TMI LWP bias, (c) SEVIRI COT, and (d) SEVIRI 1.6-μm CER.

MODIS Terra and Aqua values are also plotted. Rain-, ice-, and smoke-free conditions were applied.
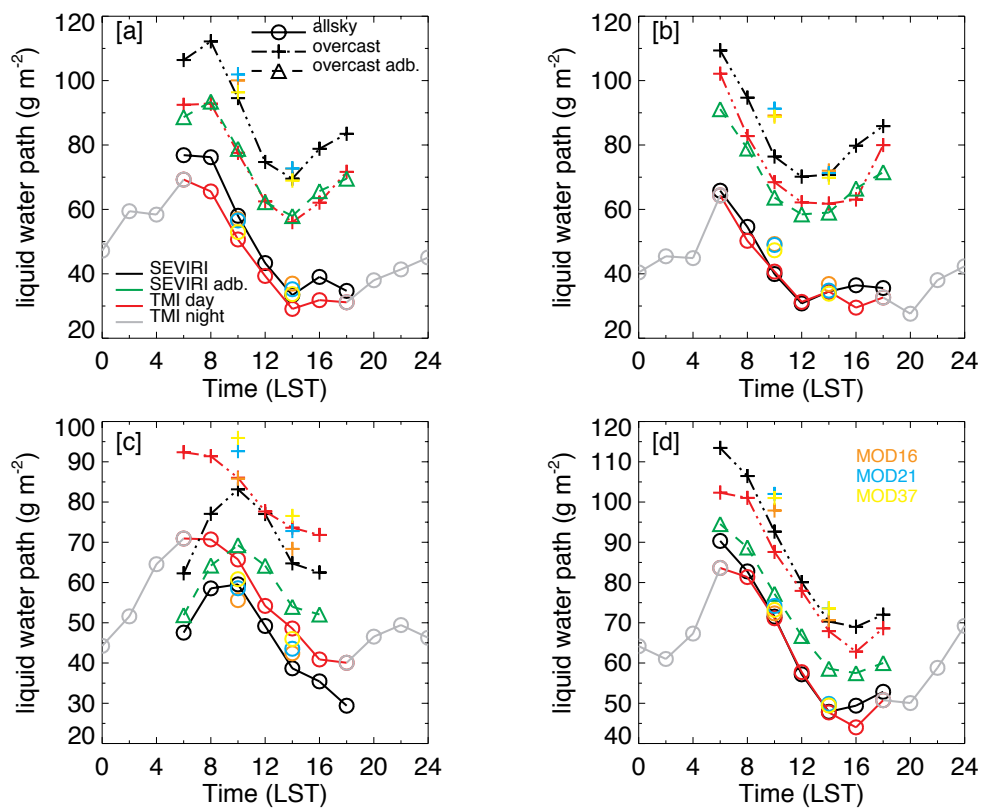
990

995

1000 **Figure 7.** Seasonal mean diurnal cycle of SEVIRI and TMI LWPs over the Sc region, both for all-sky and overcast (LCF ≥ 95% and COT > 3) cases: (a) DJF, (b) MAM, (c) JJA, and (d) SON for December 2010 to November 2012. MODIS Terra and Aqua values are also plotted. Rain-, ice-, and smoke-free conditions were applied.